Inorganic Chemistry

Article

pubs.acs.org/IC

# $H_2$azapa: a Versatile Acyclic Multifunctional Chelator for $^{67}$Ga, $^{64}$Cu, $^{111}$In, and $^{177}$Lu

Gwendolyn A. Bailey,[†,∥] Eric W. Price,[†,‡,∥] Brian M. Zeglis,[⊥] Cara L. Ferreira,[§] Eszter Boros,[†,‡] Michael J. Lacasse,[†] Brian O. Patrick,[†] Jason S. Lewis,[⊥] Michael J. Adam,*[,‡] and Chris Orvig*[,†]

[†]Medicinal Inorganic Chemistry Group, Department of Chemistry, University of British Columbia, 2036 Main Mall, Vancouver, British Columbia V6T 1Z1, Canada

[‡]TRIUMF, 4004 Wesbrook Mall, Vancouver, British Columbia V6T 2A3, Canada

[§]Nordion, 4004 Wesbrook Mall, Vancouver, British Columbia V6T 2A3, Canada

[⊥]Memorial Sloan-Kettering Cancer Center (MSKCC), Memorial Hospital, 1275 York Avenue, New York, New York 10065, United States

Supporting Information

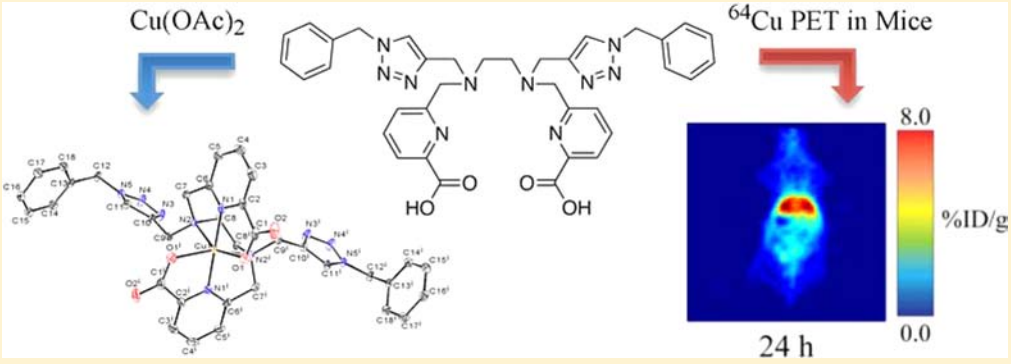


**ABSTRACT:** Preliminary experiments with the novel acyclic triazole-containing bifunctional chelator $H_2$azapa and the radiometals $^{64}$Cu, $^{67}$Ga, $^{111}$In, and $^{177}$Lu have established its significant versatile potential as an alternative to 1,4,7,10-tetraazacyclododecane-1,4,7,10-tetraacetic acid (DOTA) for metal-based radiopharmaceuticals. Unlike DOTA, $H_2$azapa radiolabels quantitatively with $^{64}$Cu, $^{67}$Ga, $^{111}$In, and $^{177}$Lu in 10 min at room temperature. In vitro competition experiments with human blood serum show that $^{64}$Cu remained predominantly chelate-bound, with only 2% transchelated to serum proteins after 20 h. Biodistribution experiments with [$^{64}$Cu(azapa)] in mice reveal uptake in various organs, particularly in the liver, lungs, heart, intestines, and kidneys. When compared to $[^{64}Cu(DOTA)]^{2-}$, the lipophilic neutral [$^{64}$Cu(azapa)] was cleared through the gastrointestinal tract and accumulated in the liver, which is common for lipophilic compounds or free $^{64}$Cu. The chelator $H_2$azapa is a model complex for a click-based bifunctional chelating agent, and the lipophilic benzyl "place-holders" will be replaced by hydrophilic peptides to modulate the pharmacokinetics and direct activity away from the liver and gut. The solid-state molecular structure of $[In(azapa)(H_2O)][ClO_4]$ reveals a very rare eight-coordinate distorted square antiprismatic geometry with one triazole arm bound, and the structure of [$^{64}$Cu(azapa)] shows a distorted octahedral geometry. The present study demonstrates significant potential for bioconjugates of $H_2$azapa as alternatives to DOTA in copper-based radiopharmaceuticals, with the highly modular and "clickable" molecular scaffold of $H_2$azapa easily modified into a variety of bioconjugates. $H_2$azapa is a versatile addition to the "pa" family, joining the previously published $H_2$dedpa ($^{67/68}$Ga and $^{64}$Cu), $H_4$octapa ($^{111}$In, $^{177}$Lu, and $^{90}$Y), and $H_5$decapa ($^{225}$Ac) to cover a wide range of important nuclides.

## INTRODUCTION

There is currently strong interest in the development of new and efficient chelators that form stable complexes with the burgeoning variety of radiometal isotopes applicable for diagnostic imaging and targeted radiotherapy, such as $^{67/68}$Ga, $^{111}$In, $^{64/67}$Cu, $^{86/90}$Y, $^{177}$Lu, $^{225}$Ac, $^{213}$Bi, $^{212}$Pb, and $^{89}$Zr.[1,2] Radioisotopes that are readily available from commercial generators and/or small cyclotrons, such as the positron emission tomography (PET) isotopes $^{64}$Cu, $^{68}$Ga, and $^{89}$Zr and the single photon emission computed tomography (SPECT) isotopes $^{111}$In, $^{67}$Ga, and $^{99m}$Tc have practical value for widespread clinical use. In light of recent recurrent global shortages of $^{99}$Mo, the parent isotope of the clinically important diagnostic nuclide $^{99m}$Tc, proper utilization of these "non-standard" isotopes is of increasing importance.[3] Radiometals

Received: October 11, 2012
Published: October 29, 2012

  

**Chart 1. Structures of Selected State-of-the-Art "Gold Standard" Chelators, and Chelators Studied or Discussed in This Work**

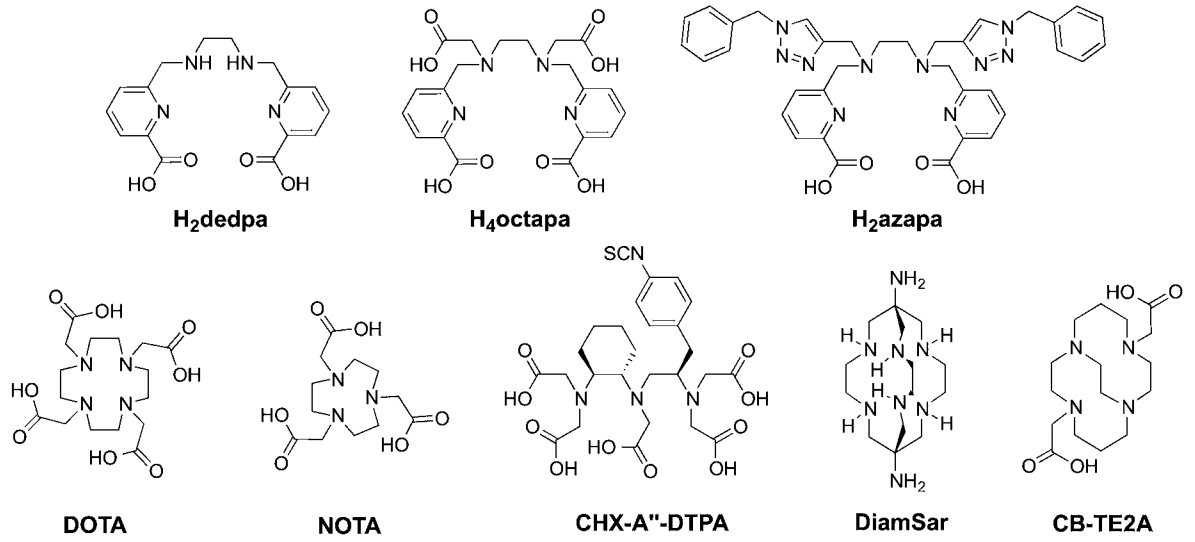


that emit particle radiation ($\beta^-/\alpha$) have intermediate (12−240 h) half-lives suitable for targeted radiotherapy, and $\beta^+$ emissions for diagnostic imaging and dosimetry calculations ("theranostic" isotopes) are of very high utility in cancer patients.[4−7] One isotope that fits into this class is $^{64}$Cu ($t_{1/2}$ = 12.7 h; $\beta^+$: 656 KeV, 19%; $\beta^-$: 573 KeV, 40%), which is made especially attractive because of the existence of imaging and/or therapeutic surrogate isotopes with complementary half-lives and decay properties that can be used in combination because of their identical chemical properties and inherent interchangeability (e.g., $^{67}$Cu: $t_{1/2}$ = 61.9 h, $\beta^-$: 395−577 KeV, 100%).[4−7]

Contemporary research in the field of receptor-based radiopharmaceutical targeting has focused almost exclusively on bifunctional chelators (BFCs) based on the tetraazamacrocyclic polycarboxylates and derivatives of the acyclic diethylenetriamine pentaacetic acid (DTPA) scaffold (Chart 1). 1,4,7,10-Tetraazacyclododecane-1,4,7,10-tetraacetic acid (DOTA) has historically been applied as an effective chelator for a variety of radiometals, including isotopes of Cu(II), Ga(III), Y(III), In(III), and Lu(III), while 1,4,7-triazacyclononane-1,4,7-triacetic acid (NOTA) is the current benchmark chelator for Ga(III) and is also very stable with Cu(II). The downside to macrocycles like DOTA is the heating typically required for quantitative radiolabeling; additionally, despite its widespread clinical and preclinical use the instability of DOTA with radioisotopes of copper has been well-documented.[2,8−11] The second-generation DTPA derivative, CHX-A′′-DTPA (Chart 1), chelates radioisotopes of Y(III), In(III), Lu(III), and Bi(III) with improved stability compared to DTPA, and although typically not as inert as DOTA in vivo, bifunctional conjugates of CHX-A′′-DTPA have shown great promise for antibody labeling with these four radiometals.[12−16] The quest for the ideal BFC for copper has been particularly challenging because of the facile ligand exchange kinetics and biologically accessible redox chemistry of Cu(II), but the availability of a selection of copper radioisotopes ($^{60/61/62/64/67}$Cu) with useful properties for therapy and imaging diagnosis/dosimetry drives basic research and development. The cross-bridged macrocycle CB-TE2A (Chart 1) is a Cu(II) chelator with exceptional stability in acid decomplexation experiments[17] and unparalleled in vivo inertness,[9,10,18] but it requires unsuitably harsh conditions (1−2 h at 95 °C) for radiolabeling. Alternatively, the sarcophagine chelators (e.g., DiamSar), NOTA, and recently developed methylphosphonate analogues of CB-TE2A (CB-TE1A1P and CB-TE2P) can be efficiently labeled at reduced temperatures.[19−22] While investigation of these chelators as bifunctional conjugates remains in its infancy, preliminary biodistribution studies have shown the unconjugated chelate-radiometal complexes to have slightly reduced stabilities compared to CB-TE2A, as evinced by their increased accumulation and slower clearance from the kidney, liver, and bone marrow over 24 h.[19−22] A new Tyr$^3$-octreotide conjugate of CB-TE1A1P has shown promise as it is radiolabeled with Cu under mild conditions (40 °C over 1 h) and offers similar in vivo performance to CB-TE2A conjugates.[23]

Our group has been investigating a new class of acyclic chelators based on the pyridinecarboxylate scaffold (Chart 1) as alternatives to the current chelator offerings that are used for radiometals of strong practical significance in nuclear medicine. Our interest in the scaffold originated in the identification of $H_2$dedpa,[24] an acyclic chelator with optimal properties for $^{68}$Ga and one of the first acyclic Ga(III) chelators known to combine the advantages of efficient room temperature labeling and excellent in vivo stability, as revealed by the rapid organ and blood clearance and low uptake in the bone during biodistribution studies in mice.[24,25] Since then, we have been making new additions to the "pa" family by derivatizing the pyridinecarboxylate scaffold to make bifunctional conjugates of $H_2$dedpa, synthesizing chelators like $H_4$octapa and $H_5$decapa with improved and tunable properties for radioisotopes of In(III), Y(III), Lu(III), Re, Tc, and Cu(II), and evaluating small, cationic, lipophilic tracers for perfusion-based cardiac PET applications with $^{68}$Ga.[24,26−30] Several bifunctional analogues of pyridinecarboxylate ligands have been prepared using the *para*-nitrobenzyl functionality as precursor to an isothiocyanate (NCS) linker (Chart 1); however, the cumbersome synthesis of backbone-derivatized $H_2$dedpa conjugates, together with the decreased efficiency of *N,N′*-ethylenediamine derivatized bifunctional constructs with $^{67/68}$Ga, has motivated a need for new conjugation methods and improved synthetic routes.[24,26]

Through our work to build on the pyridinecarboxylate-based chelator $H_2$dedpa we required new and efficient ways of functionalizing the scaffold toward biovector (e.g., peptides and


dx.doi.org/10.1021/ic302225z | Inorg. Chem. 2012, 51, 12575−12589

**Scheme 1. Synthesis of $H_2$azapa: Reagents and Conditions**[a]

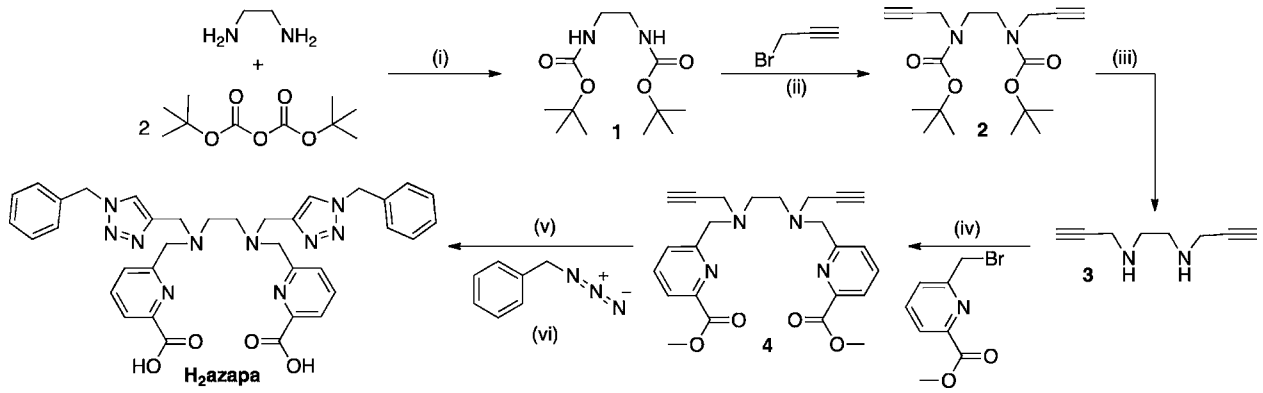


[a](i) THF, RT, 3 h; (ii) Propargyl bromide, NaO$^t$Bu, TBAI, MeCN, 0 °C−RT, 48 h; (iii) 2:1 DCM/TFA, RT, 1 h; (iv) Methyl 6-bromomethyl picolinate, $Na_2CO_3$, MeCN, RT, 48 h; (v) $BnN_3$, sodium ascorbate (0.2 equiv), $Cu(OAc)_2$ (2.1 equiv), 1:1 *t*-BuOH/$H_2O$, RT, 16 h; (vi) $Na_2S$, 1:1 THF/$H_2O$, 24 h.

antibodies) conjugation. To this end, we were interested in a "click" approach toward functionalization through incorporation of 1,2,3-triazole rings that could be synthesized via the Huisgen 1,3-dipolar cycloaddition ("click" reaction) of alkynes and azides. The model chelator $H_2$azapa (Chart 1) was designed as an elaboration of the "click-to-chelate" approach pioneered by Mindt and co-workers for the construction and conjugation of a BFC in a single, easy step[31,32] since the triazole rings would serve not only as convenient linkers between the chelator and biovectors but also as chelating arms toward the coordination sphere of large metal ions such as In(III), Y(III), and Lu(III). Benzyl groups are employed as placeholders for biological targeting vectors in the model chelator to facilitate easy synthesis, characterization, and study of the metal complexes. Herein we report the synthesis and characterization of $H_2$azapa, a novel and bifunctional triazole-containing acyclic chelator with promising characteristics for copper radiopharmaceuticals. The complexation behavior of $H_2$azapa with nonradioactive In(III), Ga(III), and Lu(III) was studied by NMR spectroscopy, and crystal structures of [In(azapa)-($H_2O$)][$ClO_4$] and [Cu(azapa)] are presented. Radiolabeling and serum stability experiments were performed with $^{67}$Ga, $^{111}$In, $^{64}$Cu, and $^{177}$Lu, and biodistribution experiments and PET imaging were performed in healthy nude athymic mice with [$^{64}$Cu(azapa)].

## RESULTS AND DISCUSSION

**Synthesis and Characterization.** The bifunctional chelator $H_2$azapa was synthesized according to a reaction scheme that was designed to improve on a previously reported method to synthesize $H_4$octapa (Chart 1, Scheme 1) and a number of pyridinecarboxylate ligands in our current chelator library.[28] The previous strategy to synthesize $H_4$octapa involved benzyl protection of the primary amines on ethylenediamine (en) using a simple reductive amination with benzaldehyde followed by alkylation with two equivalents of *tert*-butyl bromoacetate, and then benzyl deprotection to facilitate subsequent alkylation with methyl 6-(bromomethyl)-picolinate.[28] The main disadvantage to this method is that the hydrogenation reaction to remove the benzyl protecting groups is not satisfactory in the presence of olefin, alkyne, or picolinate substituents; the hydrogenation of *N,N′*-dibenzyl-*N,N′*-bis[6-(methoxycarbonyl)pyridin-2-yl]methyl-1,2-diaminoethane resulted in nonselective cleavage of both benzyl and picolinate substituents from the en amines, although various hydrogenation conditions (methanol or acetic acid as a solvent, varying catalyst loading, varying concentration) were attempted.

Thinking ahead to potential challenges that could be encountered during scale-up and commercialization of a BFC, we pursued a protecting group strategy for the synthesis of $H_2$azapa that would be fast, easy, versatile, and high-yielding with maximal purity, and also tunable for the synthesis of a library of chelators bearing picolinate, acetate, triazole, and other arms on a selection of alkylamino backbones. To this end, a novel *N,N′-tert*-butoxycarbonyl (boc) protecting group strategy was employed (Scheme 1), which relied on a carbamate alkylation reaction of the boc-protected intermediate **1** by propargyl bromide, based on a similar but noncompatible carbamate alkylation described in the literature (no reaction occurred following literature protocols).[33] This strategy led to the successful synthesis of the alkyne precursor to $H_2$azapa **4** in six steps from commercially available ethylenediamine and 2,6-pyridinedicarboxylate methyl ester, the precursor to methyl 6-(bromomethyl)picolinate, in 10% cumulative yield, which is a slight improvement over the synthetically analogous (but noncompatible) previously applied *N*-benzyl protection strategy toward the fully protected ligand precursor to $H_4$octapa.[28] For the carbamate alkylation, a nontrivial variant of a literature protocol[33] was performed, since it was found that working with an insoluble, non-nucleophilic base (NaO$^t$Bu) in a polar enolizable solvent (acetonitrile) afforded principally product, whereas other conditions attempted *ad hoc* or from the literature (e.g., combinations of bases such as $Cs_2CO_3$/$Na_2CO_3$/$K_2CO_3$/KOtBu/NaOH and solvents such as DMF/THF/*t*BuOH/MeOH) resulted in uncontrolled carbamate alkylations and deprotections with no evidence of product formation. In the carbamate deprotection step, attempts to extract the free amine from a saturated $NaHCO_3$ solution were exceptionally inefficient (25 × 1 mL extractions), although they eventually led to the isolation of product in 87% yield.

During the synthesis of the $H_2$azapa alkyne precursor **4** reported herein, it was found that the boc protecting group strategy was a slight improvement over the benzyl protection strategy used for the synthesis of $H_4$octapa and related chelators, both in terms of the simplicity of the synthetic protocols and the overall yield of the synthesis. A drawback was


dx.doi.org/10.1021/ic302225z | *Inorg. Chem.* 2012, 51, 12575−12589

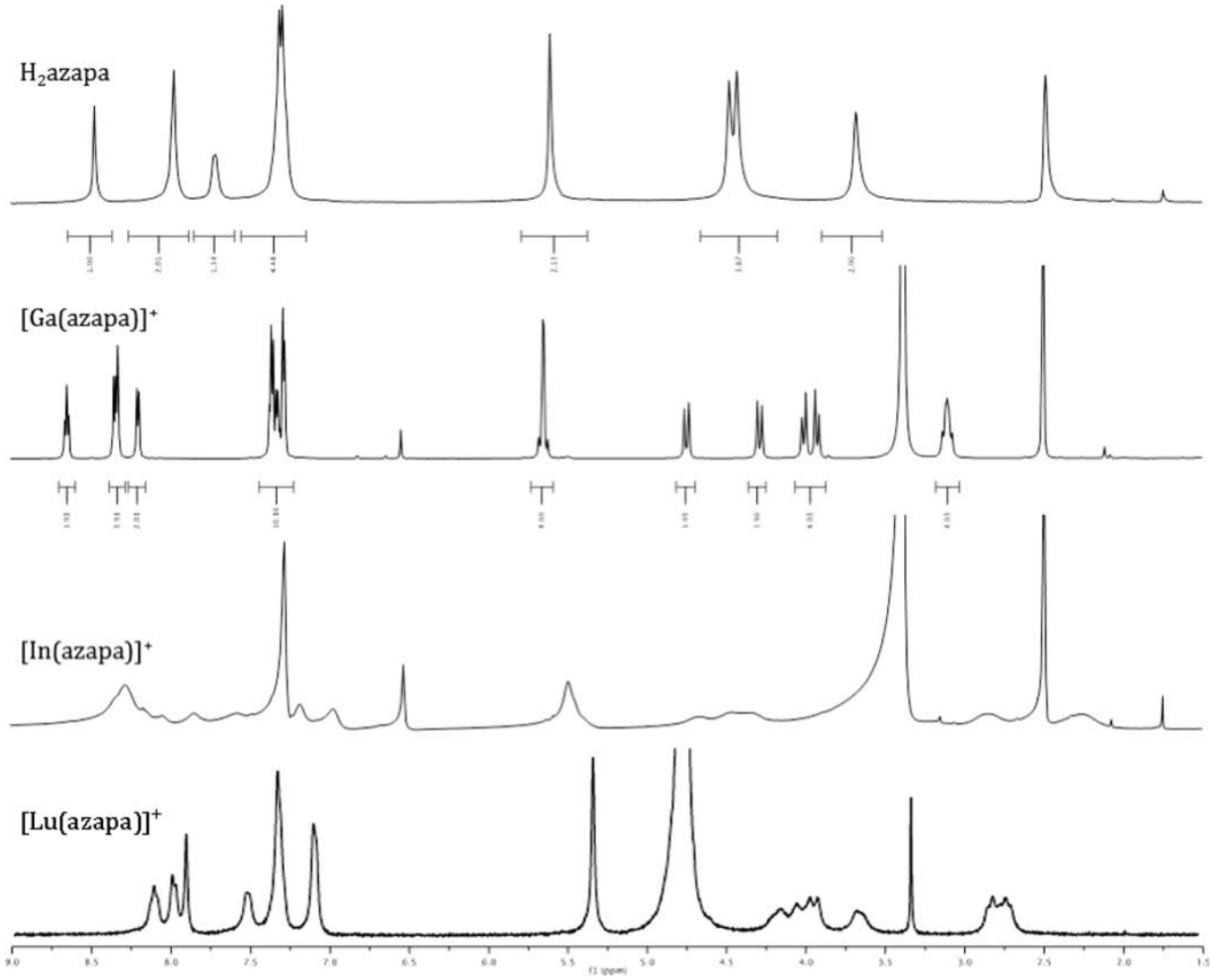


**Figure 1.** $^{1}$H NMR spectra (DMSO-$d_6$, 25 °C) of (top) $H_2$azapa, 300 MHz; (middle) $[Ga(azapa)]^+$, 600 MHz; (middle) $[In(azapa)]^+$, 400 MHz; and (bottom, 300 MHz, $D_2O$) $[Lu(azapa)]^+$, showing simple diastereotopic splittings for a single isomer of $[Ga(azapa)]^+$ and major peak broadening for solution fluxional interconversion between multiple isomers of $[In(azapa)]^+$ and, to a lesser extent, $[Lu(azapa)]^+$.

the time required for the synthesis (minimum 7 days), although this could conceivably be reduced through optimization. Unfortunately, attempts to react 1,2-di-*tert*-butylethane-1,2-dicarbamate (**1**) with *tert*-butylbromoacetate or methyl 6-(bromomethyl)picolinate did not result in the formation of product; instead the intact starting material was reisolated in quantitative yield, and it appears this reaction is only efficient with propargyl bromide as the electrophile. It is likely that the scope of the carbamate alkylation reaction is limited by the reactivity of the alkyl halides, where propargyl halide > acetyl halide > picolinyl alkyl halide. Ongoing investigation is currently underway in our laboratories to develop an improved protecting group strategy that would be applicable to all ligands in our current chelator library and provide simple and high yielding access to both "naked" chelators and their bifunctional derivatives.

The reaction of **4** with two equivalents of benzyl azide in the presence of Cu(I) generated in situ by the reduction of $Cu(OAc)_2$ with catalytic sodium ascorbate resulted in the formation of two 1-benzyl-1,2,3-triazole rings and, simultaneously, the quantitative deprotection of the picolinate methyl esters. The progress of the reaction could be followed by a gradual but distinct color change from brown to blue-green over the course of 4 h, after which a blue-green solid corresponding to [Cu(azapa)] could be observed to precipitate gradually out of solution. It was observed that super-stoichiometric rather than catalytic $Cu(OAc)_2$ was required to effect quantitative triazole formation and methyl ester deprotection under any reasonable time frame, possibly because of the increased reduction potential of Cu(II) when tightly bound to the six-coordinate picolinate core ($N_4O_2$) of $H_2$azapa/**4**, or the lack of free copper available to associate with the alkyne/azide click complex during the cycloaddition reaction. Stoichiometric Cu(II) may effect the picolinate methyl ester deprotection of $H_2$azapa by binding to the picolinate and *N*,*N*′-en nitrogen atoms of the molecule and interacting with the lone pairs on nearby carbonyl oxygen atoms to weaken the double bonds, making them susceptible to nucleophilic attack by an incoming water molecule.[34] In addition, lowering the p$K_a$ of aqua ligands bound to the *N*,*N*′-en-Cu(II) complex may facilitate the production of hydroxide species in close proximity to the methyl esters, resulting in ester cleavage.[34] After initial


dx.doi.org/10.1021/ic302225z | *Inorg. Chem.* 2012, 51, 12575−12589

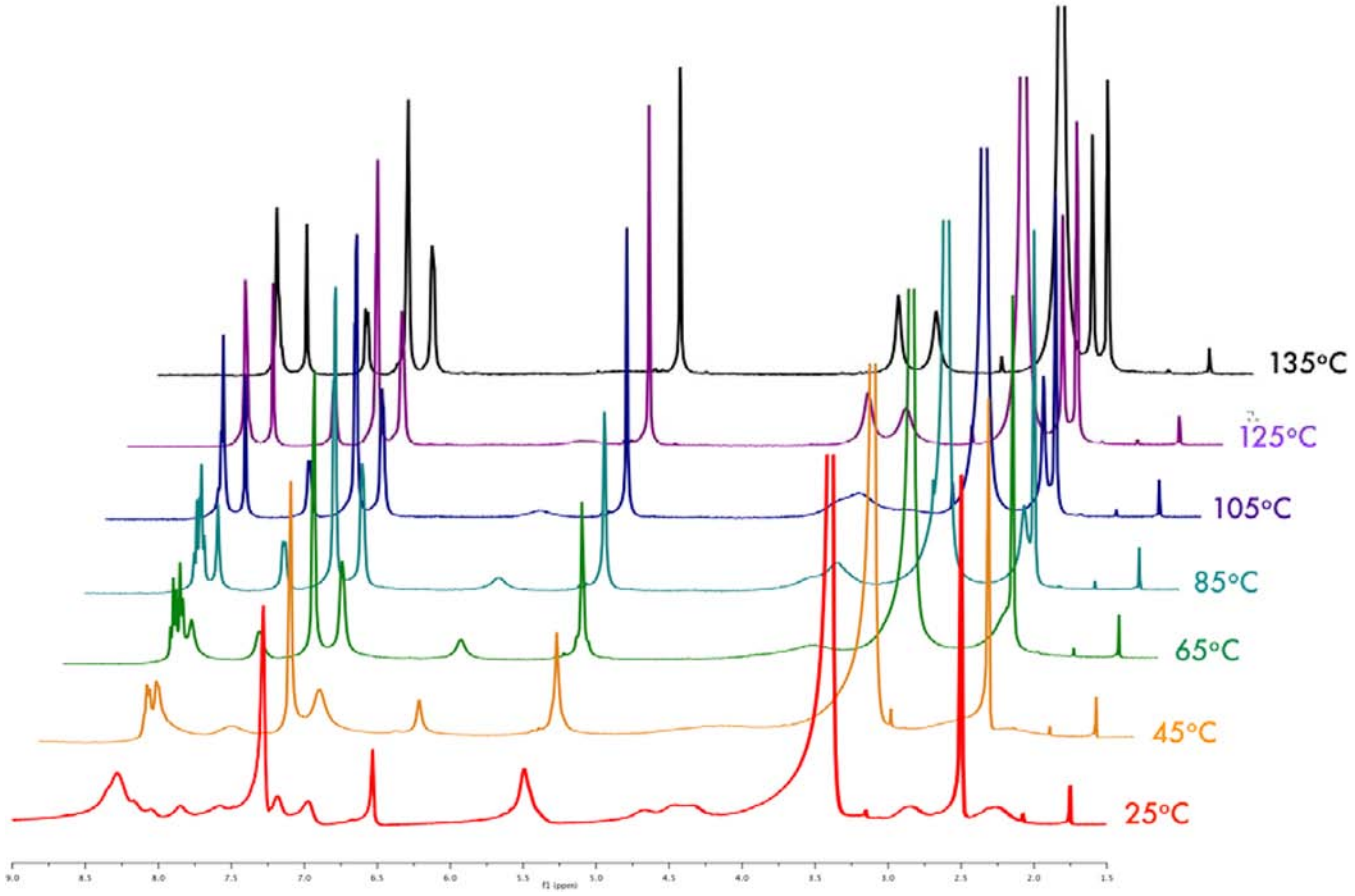


**Figure 2.** Overlay of $^{1}$H NMR spectra of [In(azapa)]$^{+}$ (400 MHz, DMSO-$d_6$) at temperatures ranging from 25 to 135 °C, showing a gradual averaging effect from increasingly rapid interconversion between multiple coordination isomers at higher temperatures.

isolation of the copper-bound chelator [Cu(azapa)] by filtration, the free chelator was liberated by reaction of the complex with an excess of $Na_2S$, which sequestered any free or bound Cu(II) as black/brown insoluble CuS that could be removed by filtration.

For receptor-targeted radiopharmaceuticals, a BFC should exhibit minimal static or fluxional isomerization in solution, since fluxional interconversion between different isomers is thought to affect in vivo stability, and static isomerization may lead to divergent biological properties, such as pharmacokinetics and biodistribution.[35−38] The simple, readily interpretable $^{1}$H NMR spectrum of [Ga(azapa)]$^{+}$ is consistent with a single isomer being present in solution (Figure 1). The spectrum shows prominent diastereotopic splittings for the methylene hydrogens associated with the picolinate and the triazole arms at 4.75/4.28 ppm ($^{2}J$ = 18 Hz) and 4.00/3.92 ppm ($^{2}J$ = 15 Hz), respectively. Methylene hydrogens on the en bridge exhibit minimal diastereotopic splitting, and are manifest in the $^{1}$H NMR spectra as a broad quartet, which is barely resolvable at 600 MHz with a chemical shift of 3.10 ppm. The benzyl methylene hydrogen atoms behave similarly, and are resolved as a sharp quartet with a characteristic downfield shift centered at 5.64 ppm. The less prominent diastereotopic splittings exhibited by the benzyl and en methylene hydrogen atoms can be explained by invoking partial flexibility in the en backbone and partial free rotation of the triazole arms extending away from the coordination center as unbound (but potentially chelating) arms. This explanation is consistent with previously reported crystal structures of the Ga(III) complex of $H_2$dedpa[24] and its nitrogen *para*-nitrobenzyl functionalized derivative, which showed highly symmetric octahedral geometries at the Ga(III) center with the six-coordinate picolinate core ($N_4O_2$) of the molecule bound in each case. Peak broadening for the en backbone methylene hydrogen atoms is also commonly observed in the $^{1}$H NMR spectra of pyridinecarboxylate ligands coordinated to metals.[24] The highly symmetric [Ga(azapa)]$^{+}$ complex has $C_2$ symmetry in solution as confirmed by the $^{13}$C NMR spectrum, which gives rise to only one signal per pair of equivalent carbon atoms on either half of the coordinated ligand.

In contrast to that of [Ga(azapa)]$^{+}$, the $^{1}$H NMR spectrum of [In(azapa)]$^{+}$ at room temperature shows a series of broad signals consistent with solution fluxional behavior commonly observed for complexes of larger trivalent metals such as In(III), Y(III), and Lu(III) with chelators of high denticities (Figure 1).[35−37] Variable temperature $^{1}$H NMR spectroscopy confirmed the solution fluxional behavior of [In(azapa)]$^{+}$ (Figure 2), as increasing the temperature of the solution stepwise from 25 to 135 °C resulted in the gradual sharpening of peaks to a series of singlets quite distinct from those observed for the free ligand (Figure 1) as the kinetics of fluxional interconversion became more rapid with increasing temperature, resulting in an overall averaging effect. Coalescence of a pair of broad signals located at 2.25 and 2.81 ppm at 25 °C can be observed at 65−85 °C, which could suggest an asymmetric, seven-coordinate structure with one triazole arm bound in solution, resulting in nonequivalence of the two pairs


dx.doi.org/10.1021/ic302225z | *Inorg. Chem.* 2012, 51, 12575−12589

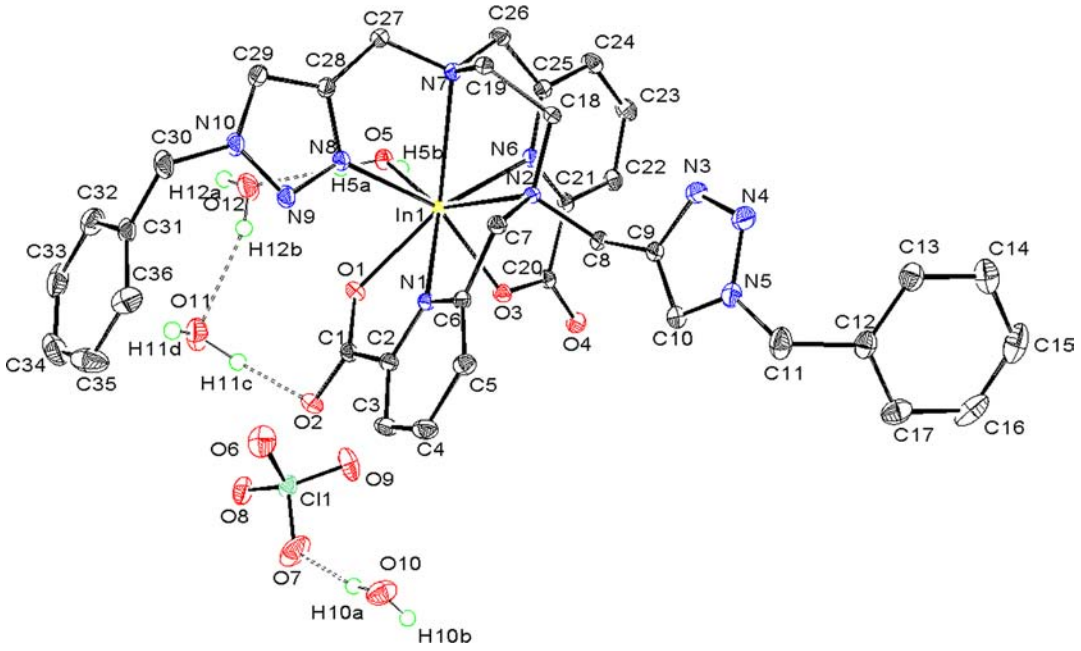


**Figure 3.** ORTEP drawing of the solid-state molecular structure of [In(azapa)($H_2O$)][$ClO_4$] obtained by X-ray diffraction. Hydrogen atoms are omitted for clarity.

of methylene hydrogens on either end of the en bridge at 25 °C.

A solid-state molecular structure of [In(azapa)($H_2O$)][$ClO_4$] was obtained by X-ray crystallographic analysis of a colorless rhombic plate crystal grown by slow evaporation of a saturated solution of 1:1 MeOH/DMSO (Figure 3). The X-ray structure reveals an eight-coordinate complex in the solid state featuring a highly distorted square antiprismatic geometry with the picolinate core, one triazole arm, and one aqua ligand bound to In(III). While six- and seven-coordinate binding modes for In(III) are common,[2] very few empirical eight-coordinate structures are known,[37,39,40] and to our knowledge [In(azapa)($H_2O$)][$ClO_4$] is the fourth such reported structure. Of the reported structures, all display distorted square antiprismatic geometries, and all are fully saturated by chelating arms.[37,39,40] Given the propensity of In(III) for seven-coordinate binding modes, an eight-coordinate structure featuring a heptadentate chelator with an additional aqua solvent ligand bound is exceptional.

The metal-to-ligand oxygen bond lengths in [In(azapa)($H_2O$)][$ClO_4$] vary between 2.216/2.320 Å for the indium-carboxylate bonds In−O(3)/O(1) and 2.219 Å for the indium-aqua ligand bond In−O(5). The indium-en backbone nitrogen bonds In−N(2)/N(7) are longer at 2.461/2.561 Å, while the indium-triazole nitrogen bond In−N(8) is the shortest of the indium−nitrogen bonds at 2.292 Å (Table 1). The In-X bond lengths for equivalent donor atoms on either side of the ligand C2 symmetry axis are similar but not identical, as is to be expected for the asymmetric heptadentate binding mode with indium. The triazole arm is bound to indium at the *N3* position of the triazole ring (see Chart 1), which is consistent with previously reported crystal structures[32,41−43] and calculated structures[44] in which the triazole chelating arm is attached to the chelator at the *C4* position of the triazole.[42,45] The relatively short In−N(8) bond in [In(azapa)($H_2O$)][$ClO_4$] is consistent with recent density functional theory (DFT) calculations[31,46,47] which suggested that a greater concentration of electron density

**Table 1. Selected Bond Angles and Lengths in the X-ray Crystal Structure of [In(azapa)($H_2O$)][$ClO_4$]**

| bond | length [Å] | angle | degree [deg] |
|---|---|---|---|
| In−O(3) | 2.216(1) | O(3)−In−O(6) | 70.25(4) |
| In−O(5) | 2.219(1) | N(6)−In−N(7) | 68.10(4) |
| In−N(8) | 2.292(1) | O(5)−In−N(6) | 76.39(4) |
| In−O(1) | 2.320(1) | O(1)−In−O(5) | 74.03(4) |
| In−N(1) | 2.303(1) | O(1)−In−N(8) | 82.89(4) |
| In−N(6) | 2.345(1) | N(2)−In−O(3) | 91.69(4) |
| In−N(2) | 2.461(1) | N(2)−In−N(8) | 97.22(4) |
| In−N(7) | 2.561(1) | O(3)−In−O(5) | 102.51(4) |

at the *N3* position of the triazole in 1,4-substituted triazoles should result in relatively strong electron donating capability to a metal center.

Since characterization using NMR spectroscopy was not feasible with the paramagnetic $d^9$ Cu(II) complex of $H_2$azapa, the bulk composition of C, N, and H in a RP-HPLC-purified batch of [Cu(azapa)] was confirmed by elemental analysis. A small, blue-green, cubic crystal of [Cu(azapa)] suitable for characterization using X-ray diffraction was grown by slow evaporation of a saturated solution of purified complex in 50% acetonitrile in water. The solid-state molecular structure of [Cu(azapa)] features a distorted octahedral metal−ligand environment typical of six-coordinate complexes of Cu(II) (Figure 4).[2] The central binding of $H_2$azapa via the picolinate ($N_4O_2$) core is typical for crystal structures reported by our group thus far for Cu(II) and Ga(III) complexes of $dedpa^{2-}$ and its bifunctional derivatives, corroborating the notion that the picolinate core of these ligands provides a versatile coordination pocket for a variety of metal ions.[24,27,30] A high degree of symmetry for these complexes, along with an approximately equally distributed set of metal−ligand bond lengths, is thought to correlate well with their high stability and favorable biological properties.[24,27] That [Cu(azapa)] is more symmetric and evenly distributed than [Cu(dedpa)],[27] and nearly as symmetric as [Ga(dedpa)][$ClO_4$][24] is belied only by


dx.doi.org/10.1021/ic302225z | *Inorg. Chem.* 2012, 51, 12575−12589

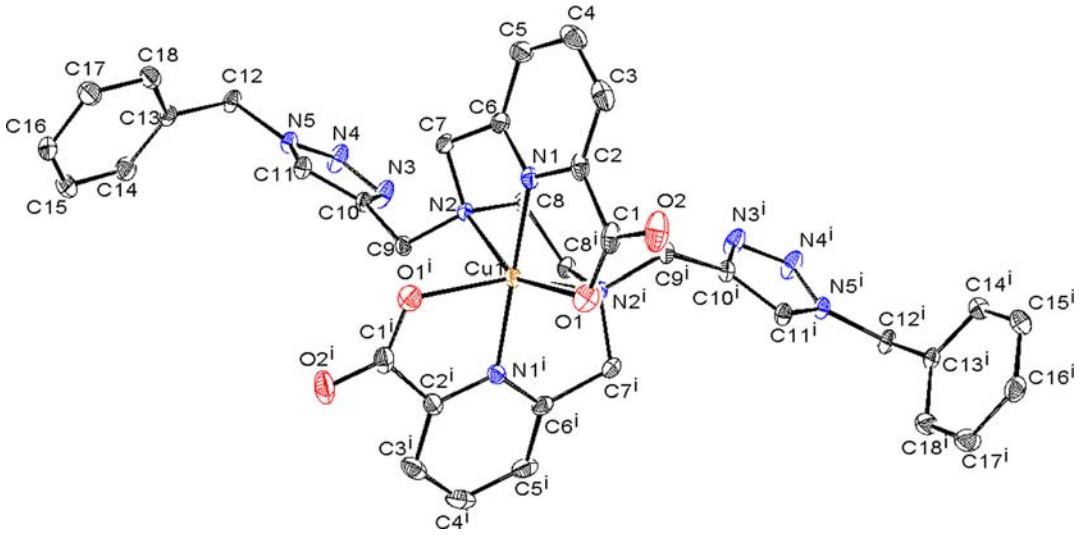


**Figure 4.** ORTEP drawing of the solid-state molecular structure of [Cu(azapa)]. Hydrogen atoms are omitted for clarity.

**Table 2. Selected Bond Angles and Lengths in the X-ray Crystal Structure of [Cu(azapa)]**[a]

| bond | length [Å] Cu(azapa) | length [Å] Cu(dedpa)[27] | length [Å] Ga(dedpa)[24] | angle | degree [deg] |
|---|---|---|---|---|---|
| Cu−N(1) | 1.935(1) | 1.9386(13) | 1.987(2) | O(3)−In−O(6) | 70.25(4) |
| Cu−N(1)$^{i}$ | ” | 2.0008(12) | 1.990(2) | N(6)−In−N(7) | 68.10(4) |
| Cu−O(1) | 2.120(1) | 2.3014(11) | 1.971(1) | O(5)−In−N(6) | 76.39(4) |
| Cu−O(1)$^{i}$ | ” | 2.0430(10) | 1.983(1) | O(1)−In−O(5) | 74.03(4) |
| Cu−N(2) | 2.326(1) | 2.1364(13) | 2.112(2) | O(1)−In−N(8) | 82.89(4) |
| Cu−N(2)$^{i}$ | ” | 2.3171(13) | 2.113(1) | N(2)−In−O(3) | 91.69(4) |

[a]Relevant bond lengths are compared to the analogous bond lengths in the previously reported X-ray crystal structure of [Ga(dedpa)]$^{+}$ and [Cu(dedpa)].[24,27]

the relatively long Cu−N(2) bond distances (Table 2), which suggest that, like in [In(azapa)][$ClO_4$] and [Ga(dedpa)][$ClO_4$], the en backbone may be somewhat loosely bound to the coordination center. The relatively long and weak Cu−N(2) bonds could conceivably facilitate attack from a biological nucleophile in vivo; on the other hand, the chelating ability of the triazole arms, which are covalently fixed to the en backbone and held in close proximity to the metal center, could also play a role in fluxional solution behavior by transiently binding Cu(II) to improve stability and inertness. Alternatively, it is conceivable that the elongated Cu−N(2) distances could be a simple result of energetic contributions from packing in the solid-state.

Potentiometric titrations of $H_2$azapa with copper were attempted so that the binding affinity (log $K_{ML}$, pM) could be determined, but the insolubility of [Cu(azapa)] obviated these experiments and cyclic voltammetry experiments. Synthesis of pegylated hydrophilic derivatives of $H_2$azapa is underway, since clickable hydrophilic polyethylene glycol (PEG) moieties should be more amenable toward aqueous experiments than the lipophilic benzyl groups of $H_2$azapa. The modular synthetic scheme for $H_2$azapa will allow for the “clickable” alkyne precursor **4** to be easily transformed into a variety of derivatives.

**Radiolabeling Experiments.** Initial radiolabeling experiments have confirmed the efficiency of $H_2$azapa to rapidly form radioactive complexes of $^{67}$Ga, $^{111}$In, $^{64}$Cu, and $^{177}$Lu quantitatively at ambient temperature in aqueous buffer (pH 4−5, NaOAc, 10 min), as determined by integration of RP-HPLC radio-traces. In contrast, DOTA required 20 min at 80 °C in a microwave reactor for quantitative labeling with $^{111}$In, and 60 min at 90 °C for $^{64}$Cu and $^{177}$Lu.[28] The single, sharp peak in the HPLC radio-traces obtained for [$^{67}$Ga(azapa)]$^{+}$ ($t_R$ = 12.8 min) and [$^{111}$In(azapa)]$^{+}$ ($t_R$ = 11.4 min) is consistent with the NMR solution structural data for these complexes, which indicate a single, robust, highly symmetric coordination isomer for [$^{67}$Ga(azapa)]$^{+}$ and rapid fluxional interconversion between multiple isomers for [$^{111}$In(azapa)]$^{+}$ on the NMR/HPLC time scale. Single peaks were also observed in the HPLC radiotraces of [$^{177}$Lu(azapa)]$^{+}$ ($t_R$ = 19.3 min) and [$^{64}$Cu(azapa)] ($t_R$ = 20.9 min) during subsequent radiolabeling experiments. RP-HPLC retention times for these radiometals indicated the increased lipophilicity of the $M^{n+}$(azapa) complexes compared to the $M^{n+}$(DOTA) and $M^{n+}$(DTPA) standards. For example, retention times for the $^{177}$Lu/$^{64}$Cu complexes of $H_2$azapa were $t_R$ = 19.3/20.9 min, and for the same complexes of DOTA they were $t_R$ = 6.8/7.1 min. The absence of free radiometal ($t_R$ ∼ 0−4 min) in the radioactive trace was confirmed in all cases by the RP-HPLC radiotraces.

**Blood Serum Stability Studies.** The serum stability data for the complexes of $H_2$azapa with $^{67}$Ga, $^{111}$In, $^{64}$Cu, and $^{177}$Lu establish $H_2$azapa as a viable and important target for further investigation with $^{64}$Cu (Table 3). [$^{64}$Cu(azapa)] displays excellent stability over the 20 h time period studied (37 °C), with less than 2% transchelated to blood serum proteins at that time, compared to [$^{64}$Cu(DOTA)]$^{2-}$, which remained only 77% and 74% intact after 1 and 20 h, respectively. The data also compare favorably to a recent report of a mouse serum competition experiment of $H_2$dedpa and a *N,N′-para*-nitrobenzyl functionalized cRGDyk conjugate,[27] $H_2$RGD-2, with


dx.doi.org/10.1021/ic302225z | *Inorg. Chem.* 2012, 51, 12575−12589

**Table 3. Stability Data Collected in Mouse Blood Serum at 25 °C for $^{67}$Ga and $^{111}$In and in Human Blood Serum with Agitation (550 rpm) at 37 °C for $^{64}$Cu and $^{177}$Lu, with $H_2$azapa and Selected Chelator Standards[a]**

| complex[b] | (a) short-term stability[b] (%) | (b) medium-term stability (%) | (c) long-term stability (%) |
|---|---|---|---|
| $[^{67}Ga(azapa)]^+$ | 69 (±2) | 48 (±2) | 52 (±4) |
| $[^{67}Ga(dedpa)]^+$ | >99 | >99 | >99 |
| $[^{67}Ga(dp\text{-}N\text{-}NO_2)]^+$ | 88 | 69 | 51 |
| $[^{67}Ga(dp\text{-}bb\text{-}NO_2)]^+$ | 98 | 97 | 97 |
| $[^{111}In(azapa)]^+$ | | 95.1 (±0.6) | 65 (±4) |
| $[^{111}In(DTPA)]^{2-}$ | | 87 (±2) | 88 (±2) |
| $[^{111}In(DOTA)]^-$ | | 90 (±2) | 89 (±2) |
| $[^{64}Cu(azapa)]$ | | 99.9 (±0.1) | 98.3 (±0.2) |
| $[^{64}Cu(DOTA)]^{2-}$ | | 77 (±6) | 74 (±1) |
| $[^{177}Lu(azapa)]^+$ | | 55 (±4) | 46 (±1) |
| $[^{177}Lu(DOTA)]^-$ | | 87.7 (±0.7) | 87 (±2) |
| $[^{177}Lu(DTPA)]^{2-}$ | | 77 (±1) | 82 (±2) |

[a]The % stability shown is the percentage of chelator-bound radiometal and the error is expressed as standard deviation ($n$ = 3). (a) Short-term stability data at 15 min for $[^{67}Ga(azapa)]^+$ and 10 min for all other complexes; (b) medium-term stability data at 1 h, except for $^{177}$Lu complexes which were at 1.5 h; (c) long-term stability data at 2 h for $^{67}$Ga complexes, 20 h for $^{64}$Cu complexes, and 24 h for $^{111}$In and $^{177}$Lu complexes. [b]Relevant data for the $^{67}$Ga complexes of $H_2$dedpa and the nitrogen and backbone *para*-nitrobenzyl functionalized $H_2$dedpa derivatives $H_2$dp-N-$NO_2$ and $H_2$dp-bb-$NO_2$ are from previously reported *apo*-transferrin challenge experiments.[24]

$^{64}$Cu in which 23% of $^{64}$Cu from $[^{64}Cu(dedpa)]$ and 12% of $^{64}$Cu from $[^{64}Cu(RGD\text{-}2)]$ was transchelated to serum proteins after 24 h at ambient temperature,[27] suggesting that $H_2$azapa is a more stable/inert chelator for copper than are $H_2$dedpa and its *N,N′*-en-nitrogen functionalized derivatives. Chelators that remain robust with isotopes of copper over a much longer time period (e.g., 24−72 h) while efficiently labeling at room temperature are highly sought to advance receptor-based targeting using antibodies and other sensitive biological vectors for PET with $^{64}$Cu and dosimetry/therapy using $^{64}$Cu/$^{67}$Cu.[48−52] Antibodies have longer biological half-lives, sluggishly distribute to target tissues, and must be labeled at reduced temperatures (20−37 °C) to avoid protein denaturation and retarded immunoreactivity and binding affinity.[49,50,53] PET using antibody targeting is typically optimized at ∼24−72 h post injection, which requires the chelate-radiometal complex to be stable over that entire time period.[54,55] Furthermore, tumor targeting for therapy using isotopes such as $^{67}$Cu, $^{177}$Lu, and $^{90}$Y require an even longer biological stability window, since the chelate-radiometal complex should be delivered to the target tumor and then remain intact until the majority of the isotope has decayed (e.g., $^{67}$Cu: $t_{1/2}$ = 61.9 h).[50,55] Kinetic inertness has been shown to be a more accurate predictor of the biological stability of chelate-radiometal complexes than thermodynamic stability,[2,9,56,57] and to date the most relevant assays for biological stability, besides in vivo experiments, are in vitro blood serum/*apo*-transferrin/superoxide dismutase competition challenges.

The blood serum stability data for chelators with $^{67}$Ga, $^{111}$In, and $^{177}$Lu reveal the stability of $H_2$azapa with each of these radiometals. The $H_2$azapa-bound $^{177}$Lu and $^{111}$In are 54% and 35% transchelated by serum proteins after 24 h, compared with our leading candidate for these radiometals, $H_4$octapa, which is >85% stable at 24 h with both $^{177}$Lu and $^{111}$In (<15% transchelated).[28] $H_2$azapa displays roughly comparable stability as a complex with $^{67}$Ga to the similar nitrogen functionalized *para*-nitrobenzyl $H_2$dedpa derivative $H_2$dp-N-$NO_2$, which was roughly 50% intact after 2 h in a similar *apo*-transferrin challenge experiment.[24] Between the quartet of $H_2$azapa, $H_2$dedpa,[24] $H_4$octapa,[28] and $H_5$decapa,[28] we have a large number of clinically relevant and high impact metal ions/isotopes well covered.

A much more demanding test of the biological stability of the chelate-radiometal complex is a biodistribution experiment in animals, where the ability of the complex to resist transchelation by native biological chelating proteins and enzymes like superoxide dismutase (SOD), serum albumin, and transferrin is ultimately tested by its effective clearance through the kidneys (ideally) and low uptake in the liver, lung, spleen,

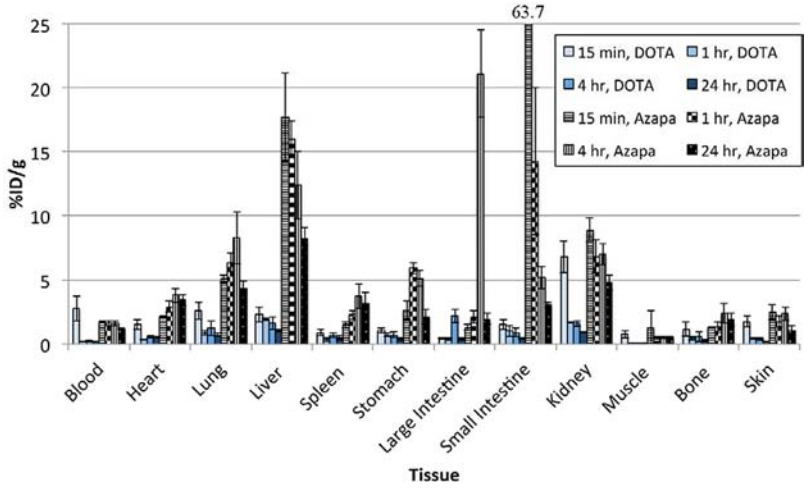


**Figure 5.** Biodistribution of $[^{64}Cu(azapa)]$ and $[^{64}Cu(DOTA)]^{2-}$ showing organ and tissue uptake as percent injected dose per gram (% ID/g) obtained over 24 h in healthy athymic nude mice; *Y*-axis is normalized at 25% ID/g for clarity.


dx.doi.org/10.1021/ic302225z | *Inorg. Chem.* 2012, 51, 12575−12589

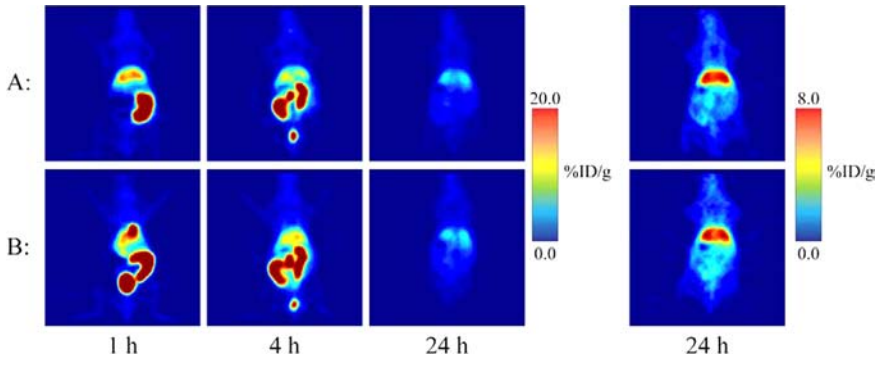


**Figure 6.** PET images of two (A and B) healthy female nude athymic mice injected with [$^{64}$Cu(azapa)] and imaged at 1, 4, and 24 h post injection, showing rapid clearance through the gut, with ~8%ID/g remaining in the liver after 24 h.

**Table 4. Biodistribution of [$^{64}$Cu(azapa)] and [$^{64}$Cu(DOTA)]$^{2-}$ in Healthy Nude Athymic Mice ($n$ = 4) Showing Organ Uptake as % ID/g, with the Error Expressed as Standard Deviation (SD), at 15 min, 1 h, 4 h, and 24 h Time Points**

| organ | 15 min (±SD) | 1 h (±SD) | 4 h (±SD) | 24 h (±SD) |
|---|---|---|---|---|
| | | [$^{64}$Cu(azapa)] | | |
| blood | 1.72 (±0.12) | 1.62 (±0.20) | 1.62 (±0.20) | 1.19 (±0.08) |
| heart | 2.12 (±0.12) | 2.91 (±0.43) | 3.81 (±0.55) | 3.44 (±0.44) |
| lung | 5.10 (±0.28) | 6.39 (±0.71) | 8.24 (±2.03) | 4.30 (±0.60) |
| liver | 17.71 (±3.48) | 15.97 (±1.43) | 12.39 (±2.64) | 8.14 (±0.94) |
| spleen | 1.50 (±0.22) | 2.27 (±0.33) | 3.72 (±0.97) | 3.13 (±0.96) |
| stomach | 2.64 (±0.75) | 5.93 (±0.43) | 5.11 (±0.62) | 2.13 (±0.58) |
| large intestine | 1.28 (±0.21) | 2.11 (±0.50) | 21.12 (±3.44) | 1.93 (±0.44) |
| small intestine | 63.73 (±26.06) | 14.28 (±5.77) | 5.18 (±0.85) | 3.05 (±0.18) |
| kidney | 8.87 (±0.93) | 6.84 (±1.28) | 6.98 (±0.77) | 4.80 (±0.60) |
| muscle | 1.27 (±1.31) | 0.45 (±0.08) | 0.47 (±0.06) | 0.48 (±0.07) |
| bone | 1.27 (±0.06) | 1.30 (±0.39) | 2.38 (±0.78) | 1.88 (±0.50) |
| skin | 2.52 (±0.59) | 1.77 (±0.45) | 2.38 (±0.54) | 1.04 (±0.36) |
| | | [$^{64}$Cu(DOTA]]$^{2-}$ | | |
| blood | 2.77 (±0.95) | 0.21 (±0.02) | 0.22 (±0.03) | 0.16 (±0.01) |
| heart | 1.53 (±0.43) | 0.37 (±0.04) | 0.57 (±0.10) | 0.52 (±0.07) |
| lung | 2.61 (±0.66) | 0.89 (±0.20) | 1.25 (±0.60) | 0.71 (±0.12) |
| liver | 2.32 (±0.61) | 1.91 (±0.07) | 1.64 (±0.50) | 1.04 (±0.10) |
| spleen | 0.90 (±0.23) | 0.34 (±0.11) | 0.69 (±0.18) | 0.48 (±0.16) |
| stomach | 1.03 (±0.21) | 0.70 (±0.17) | 0.72 (±0.20) | 0.35 (±0.10) |
| large intestine | 0.42 (±0.03) | 0.37 (±0.10) | 2.19 (±0.53) | 0.35 (±0.08) |
| small intestine | 1.53 (±0.43) | 1.01 (±0.47) | 0.88 (±0.36) | 0.44 (±0.08) |
| kidney | 6.81 (±1.22) | 1.66 (±0.07) | 1.59 (±0.20) | 0.93 (±0.05) |
| muscle | 0.72 (±0.29) | 0.09 (±0.02) | 0.09 (±0.03) | 0.09 (±0.03) |
| bone | 1.17 (±0.57) | 0.45 (±0.13) | 0.55 (±0.40) | 0.27 (±0.07) |
| skin | 1.76 (±0.47) | 0.40 (±0.04) | 0.34 (±0.11) | 0.17 (±0.03) |

kidneys, intestines, blood, and bone. The clearance and biological distribution pattern of a metal complex is dependent on the size, shape, charge, thermodynamic stability, kinetic inertness, and overall polarity of the complex, such that these same properties can be manipulated to modulate pharmacokinetics and promote effective uptake into, or away from, various organs.[30,38] It is sometimes difficult to discern whether a complex shows uptake in an organ because of its instability/transchelation to proteins within that organ (or blood), or whether the intact complex is being taken up and retained because of its physical properties. Metabolism studies, which can help identify % authentic intact (% AI) complex within a given organ vs "free" radiometal can be useful to this end.[9,10] For bifunctional chelate-based radiopharmaceuticals, the biodistribution profile is largely dominated by the properties of the attached biovector (e.g., antibody, peptide, nanoparticle), particularly in the case of large targeting vectors such as antibodies (MW~150 kDa) and antibody fragments.[18,20,24,26]

The biodistribution of [$^{64}$Cu(azapa)] shows elevated uptake in all organs compared to [$^{64}$Cu(DOTA)]$^{2-}$, particularly the liver, lung, heart, spleen, stomach, intestines, and kidneys (Figure 5). [$^{64}$Cu(azapa)] can be observed to move through the digestive tract over 24 h, with activity levels peaking at 15 min post injection in the small intestines (63.7−14.3%ID/g from 15 min to 1 h), peaking in the large intestine at 4 h (21.1%ID/g), and finally being excreted through the feces, as pictured via PET (Figure 6), confirming elimination through the digestive system (Table 4). High uptake in the stomach was also observed, with activity levels peaking at 1 h (5.6%ID/g). Although metabolism and clearance appeared to be mostly through the hepatobiliary and digestive system, there was also some kidney clearance observed, and the amount of activity decreased over 24 h in both of these organs (liver: 17.7−8.1%


dx.doi.org/10.1021/ic302225z | Inorg. Chem. 2012, 51, 12575−12589

ID/g; kidney: 8.9−4.8%ID/g, 15 min-24 h). While an increase in $^{64}$Cu uptake in the liver and kidneys is often cited as being evidence for instability of the $^{64}$Cu chelate-radiometal complex in vivo, the complex [$^{64}$Cu(azapa)] is accumulated in many other organs as well, strongly suggesting distribution of the intact lipophilic complex. DOTA in particular is known to display instability and transchelation of $^{64}$Cu in mice with bioconjugate systems,[8−11] and the differences in the biodistribution of $H_2$azapa and DOTA, particularly the elevated uptake of [$^{64}$Cu(azapa)] in the stomach, intestines, heart, and lung, suggest that the mechanism of uptake in these organs is related to the physical characteristics of the intact complex, as opposed to the instability of [$^{64}$Cu(azapa)] and resultant transchelation to proteins in these organs.

Persistent uptake in the liver, lung, heart, and gut are expected for small lipophilic molecules, and elevated uptake in the blood and kidneys is also often observed.[58−60] The pressing issue with $^{64}$Cu is that "free" or transchelated Cu(II) is known to accumulate in the liver, and highly lipophilic molecules (such as [Cu(azapa)]) are also known to accumulate in the liver and kidneys, which makes the standard assessment of stability by monitoring the amount of $^{64}$Cu accumulated in the liver problematic. Furthermore, with the high abundance of superoxide dismutase (SOD) in the liver, accumulation and retention of the intact and lipophilic [$^{64}$Cu(azapa)] complex in the liver could result in very harsh metabolic conditions and a very strict Cu(II) transchelation challenge with SOD.[56] This is in sharp contrast to the hydrophilic $[Cu(DOTA)]^{2-}$ complex, which cleared very quickly through the kidneys/bladder/urine, and since a majority of the injected activity was cleared within 15 min, the complex was not subject to the same harsh and degrading environment (liver) as [$^{64}$Cu(azapa)].

To observe a fair competition between these chelators, bioconjugates (e.g., antibody) must be synthesized and compared in vivo. The rapid clearance of high amounts of $^{64}$Cu through the digestive system, as well as its high uptake in the lungs and heart, suggest that [$^{64}$Cu(azapa)] remains intact. Recent investigation into a series of small, cationic, lipophilic derivatives of $H_2$dedpa that bore lipophilic methoxyphenyl substituents showed that with $^{67/68}$Ga the complexes that were the most stable in vitro with $^{67}$Ga, but that were concurrently the most lipophilic by RP-HPLC, displayed greatly elevated uptake in the liver, intestine, heart, and lung, although they remained stable as confirmed by low bone uptake of "free" $^{67}$Ga.[30] Uptake and clearance from the kidneys was also prominent in the biodistribution for each of these compounds, particularly those that were unstable in vitro. For comparison, Ando et al. injected $^{64}CuCl_2$ into Donryu rats with implanted sarcomas, and found that activity accumulation was highest for "free" metal in the liver and kidney,[61] while for $^{64}$Cu complexes of DOTA, TETA, and cross-bridged cyclams known to be unstable in vivo,[10,11,56] abnormal accumulation in the blood and bone was also commonly observed.[10,11,56]

The reason for elevated uptake of [$^{64}$Cu(azapa)] in various organs is difficult; however, the model ligand $H_2$azapa was never intended as a biologically relevant chelator, with its lipophilic benzyl "placeholders" being excellent for studies using standard analytical techniques but not intended for use in final radiopharmaceutical formulations. The elevated uptake of [$^{64}$Cu(azapa)] in the small intestine, large intestines, stomach, spleen, heart, and lungs suggests that the physical properties of the neutral, lipophilic complex facilitate uptake of the intact complex into these organs. This promising observation suggests that future elaborations of the $H_2$azapa scaffold as hydrophilic peptide bioconjugates will remain intact in vivo and work well as $^{64}$Cu PET imaging agents. Efforts are currently underway to synthesize hydrophilic PEG-3 and peptide conjugates of $H_2$azapa to modulate the pharmacokinetics away from the gut, liver, and lungs, when compared to $H_2$azapa, toward selective tumor uptake for imaging and therapy. It is anticipated that the propensity of [$^{64}$Cu(azapa)] toward persistent organ uptake is solely a result of its lipophilic character and not chelate instability, and the modular and "clickable" $H_2$azapa scaffold should be an excellent candidate for receptor-based targeting using larger, more sensitive biological targeting vectors like peptides and antibody fragments that require low temperature radiolabeling.

The ability of $H_2$azapa to radiolabel $^{177}$Lu, $^{111}$In, $^{67}$Ga, and $^{64}$Cu quantitatively in 10 min at ambient temperature shows impressive flexibility and versatility. It is also of interest to note that high heart uptake was observed over 24 h (uptake of 3.8% ID/g at 4 h and 3.4%ID/g at 24 h), with a heart/blood ratio of 1.9 at 1 h and 2.9 at 24 h, which is comparable to many $H_2$dedpa cardiac derivatives recently published,[30] and fortuitously suggests that a modified version of this neutrally charged Cu(II) chelator scaffold could be used for heart imaging. Further, the neutral and lipophilic physical properties of $H_2$azapa could lead to applications in tumor hypoxia imaging through decoration of the molecular scaffold with nitroimidazole functionality. The modularity of the "clickable" precursor **4** (alkyne functionalized chelator) adds a large degree of versatility to this scaffold, as many different bifunctional derivatives can be synthesized from the same precursor (e.g., peptide, antibody, antibody fragment, nanoparticle, PEG chain, nitro-imidazole), which will allow for facile and simple synthesis of these derivatives with little or no changes in synthetic methodology. $H_2$azapa provides a highly versatile and flexible molecular framework for synthesizing facile click-based bioconjugates; an important addition to the "pa" family, which currently includes the quartet of chelators $H_2$azapa, $H_2$dedpa,[24] $H_4$octapa,[28] and $H_5$decapa,[28] and covers a wide base of radiometal ions for imaging and therapy applications.

## ■ CONCLUSIONS

We have presented the synthesis, characterization, complexation, and radiolabeling of $H_2$azapa, the first known example of a bifunctional triazole-containing acyclic chelator based on a "clickable" version of the pyridinecarboxylate scaffold. Besides investigating its complexation and stability properties with a selection of radiometals of current interest in nuclear medicine, we were interested to investigate the feasibility of an alternative "click" approach toward biovector conjugation and derivatization of the scaffold toward potentially higher denticity systems with larger metals such as In(III), Y(III), and Lu(III). Our hypothesis was that the formation of robust, coordinatively saturated complexes in the solution phase would result in kinetically inert chelate-radiometal complexes in vivo.

From our preliminary investigation, $H_2$azapa appears to be a viable candidate as a "clickable" bifunctional chelator for copper radiopharmaceuticals, and a valuable addition to the "pa" family of chelators ($H_2$dedpa, $H_4$octapa, and $H_5$decapa). This is demonstrated by the ability of $H_2$azapa to quantitatively radiolabel $^{64}$Cu in 10 min at ambient temperature in aqueous buffer (pH 4−5), and by its robust inertness in human blood serum, in which it shows only 2% transchelation by serum proteins after a 20 h incubation period. This is in stark contrast

to DOTA, which required elevated temperatures for radiolabeling and was only 74% intact after 20 h incubation period with human blood serum, further substantiating its nonoptimal properties for both antibody and peptide labeling with $^{64}$Cu. The solid-state molecular structure of [$^{64}$Cu(azapa)] confirmed a coordinatively saturated six-coordinate structure with the picolinate ($N_4O_2$) core of the molecule bound and the triazole arms extending away from the metal ion center. Although the In(III) complex of $H_2$azapa was unstable in serum and was not further investigated in vivo, it formed a highly unusual and rare eight-coordinate complex with In(III) showing coordination to the picolinate core, one triazole arm, and one aqua ligand, one of only a handful of 8-coordinate In(III) complexes.

Despite the high stability of [$^{64}$Cu(azapa)] in the presence of biological serum proteins, uptake in a variety of organs, notably the liver, stomach, intestines, and kidneys was observed in nude athymic mice, most likely because of its neutrally charged and highly lipophilic physical properties. [$^{64}$Cu(azapa)] cleared from the liver and passed through the intestines and gut relatively rapidly in mice, with ~8% ID/g remaining in the liver after 24 h; however, persistent uptake in the liver, lung, heart, and gut are expected for small, lipophilic molecules, and $H_2$azapa is merely a model ligand designed for preliminary study. [$^{64}$Cu(azapa)] demonstrated exceptional stability compared to [$^{64}$Cu(DOTA)]$^{2-}$ in serum, and the uptake of [$^{64}$Cu(azapa)] in organs and tissues can be explained by the high lipophilicity of the intact, neutral complex, which suggests great potential for future elaboration with hydrophilic peptide biovectors. The modular design of this "clickable" system will facilitate the fast and simple synthesis of a number of new derivatives. Further investigation into the biological stability of bifunctional bioconjugates of $H_2$azapa exploiting hydrophilic peptides and PEG groups will likely secure the potential of $H_2$azapa as a useful bifunctional chelator for copper.

## EXPERIMENTAL SECTION

**Materials and Methods.** All solvents and reagents were purchased from commercial suppliers (Sigma Aldrich, St. Louis, MO; TCI America, Portland, OR; Fisher Scientific, Waltham, MA) and were used as received unless otherwise indicated. Methyl 6-(bromomethyl)picolinate was synthesized according to a literature protocol.[28] Water used was ultrapure (18.2 MΩ cm$^{-1}$ at 25 °C, Milli-Q, Millipore, Billerica, MA). The analytical thin-layer chromatography (TLC) plates were aluminum-backed ultrapure silica gel (Siliaplate, 60 Å pore size, 250 μM plate thickness, Silicycle, Quebec, QC). Flash column silica gel was provided by Silicycle (Siliaflash Irregular Silica Gels F60, 60 Å pore size, 40−63 mm particle size, Silicycle, Quebec, QC). Automated column chromatography was performed using a Teledyne Isco (Lincoln, NE) CombiFlash $R_f$ automated system with solid load cartridges packed with flash column silica gel and RediSep $R_f$ Gold reusable normal-phase silica columns (Teledyne Isco, Lincoln, NE). $^1$H and $^{13}$C NMR spectra were recorded on Bruker AV300, AV400, or AV600 instruments; all spectra were internally referenced to residual solvent peaks except for $^{13}$C NMR spectra in $D_2O$, which were externally referenced to a sample of $CH_3OH/D_2O$. Low-resolution mass spectrometry was performed using a Waters liquid chromatography−mass spectrometer (LC-MS) consisting of a Waters ZQ quadrupole spectrometer equipped with an ESCI electrospray/chemical ionization ion source and a Waters 2695 HPLC system (Waters, Milford, MA). High-resolution electrospray-ionization mass spectrometry (EI-MS) was performed on a Waters Micromass LCT time-of-flight instrument. Microanalysis for C, H, and N was performed on a Carlo Erba EA 1108 elemental analyzer. The HPLC system used for purification of nonradioactive compounds consisted of a semipreparative reverse phase C18 Phenomenex synergi hydro-RP (80 Å pore size, 250 × 21.2 mm, Phenomenex, Torrance, CA) column connected to a Waters 600 controller, a Waters 2487 dual wavelength absorbance detector, and a Waters delta 600 pump. Radiochemical experiments with $^{67}$Ga and $^{111}$In were performed at TRIUMF/Nordion in Vancouver, BC. $^{67}$Ga and $^{111}$In were cyclotron produced (Advanced Cyclotron Systems, Model TR30) by proton bombardment through the reactions $^{68}$Zn($p$,2$n$)$^{67}$Ga and $^{111}$Cd($p$,$n$)$^{111}$In and provided by Nordion as $^{67}GaCl_3$ and $^{111}InCl_3$ solutions in 0.05 M HCl. Analysis of radiolabeled compounds was performed using an analytical HPLC system consisting of a Waters xbridge BEH130 C18 reverse phase (150 × 6 mm) analytical column and a Waters Alliance HT 2795 separation module equipped with a Raytest Gabi Star NaI (Tl) detector (Raytest GmbH, Straubenhardt, Germany) and a Waters 996 photodiode array (PDA) detector. Blood serum competition experiments with $^{67}$Ga/$^{111}$In were performed using previously frozen mouse blood serum (Sigma, M5905−5 mL). Blood serum competition solutions were analyzed using GE Healthcare Life Sciences PD-10 desalting columns (GE Healthcare, United Kingdom, MW < 5000 Da filter) conditioned by elution of 20 mL of phosphate-buffered saline (PBS) before use. Radioactivity counting for $^{67}$Ga and $^{111}$In was performed using a Capintec CRC 15R dose calibrator (Capintec, Ramsey, NJ).

Radiochemical experiments with $^{177}$Lu and $^{64}$Cu were performed at Memorial Sloan-Kettering Cancer Center (MSKCC) in New York and utilized the following materials and methods. $^{177}$Lu was procured from Perkin-Elmer (Perkin-Elmer Life and Analytical Sciences, Wellesley, MA, effective specific activity of 29.27 Ci/mg) as $^{177}LuCl_3$ in 0.05 M HCl. $^{64}$Cu was purchased from Washington University, St. Louis (Washington University School of Medicine Cyclotron, model CS-15, Cyclotron Corp., $^{64}$Ni($p$,$n$)$^{64}$Cu) and purified as previously described to yield [$^{64}$Cu]$CuCl_2$ with an effective specific activity of 200−400 mCi/μg (7.4−14.8 GBq/μg).[62] All radiolabeling chemistry was performed with ultrapure water (>18.2 MΩ cm$^{-1}$ at 25 °C, Milli-Q, Millipore, Billerica, MA) which had been passed through a 10 cm column of Chelex resin (BioRad Laboratories, Hercules, CA). The HPLC used was a Shimadzu SPD-20A prominence UV/vis, LC-20AB prominence LC, a Bioscan flow-count radiation detector, and a C18 reverse phase column (Phenomenex Luna Analytical 250 × 4.6 mm). Blood serum competition experiments with $^{64}$Cu/$^{177}$Lu were performed using human blood serum (Sigma, Sera, human, aseptically filled, S7023−100 mL). Human blood serum competition solutions were agitated at 550 rpm and held at 37 °C using an Eppendorf Thermomixer and then analyzed using GE Healthcare Life Sciences PD-10 desalting columns as described above for $^{67}$Ga and $^{111}$In serum competition solutions. Radioactivity in samples was measured using a Capintec CRC-15R dose calibrator (Capintec, Ramsey, NJ), and for biodistribution studies a Perkin-Elmer (Waltham, MA) Automated Wizard Gamma Counter was used for counting organ activities and creating calibration curves. PET imaging was performed using a micro-PET R4 rodent scanner (Concord Microsystems).

**Di-*tert*-butyl Ethane-1,2-dicarbamate (1).** To a solution of ethylenediamine (770 μL, 11.5 mmol) in tetrahydrofuran (THF, 60 mL) was added dropwise a solution of di-*tert*-butyl dicarbonate (5.449 g, 25.0 mmol, 2.2 equiv) in THF (10 mL). A white solid precipitated immediately. The resulting white suspension was stirred under argon at ambient temperature and monitored by TLC and EI-MS. TLC showed the gradual disappearance of *tert*-butyl dicarbonate ($R_f$: 0.65, TLC in 25% EtOAc in hexanes/$KMnO_4$ staining) in favor of product ($R_f$: 0.25). After 3 h the reaction mixture was concentrated in vacuo to dryness, and the resulting white solid was redissolved in dichloromethane (100 mL). The organic layer was washed with water (2 × 20 mL) and brine (1 × 20 mL). The combined aqueous layers were dried ($MgSO_4$), filtered, and concentrated in vacuo to dryness. The resulting colorless solid was dissolved in a minimum volume (~5 mL) of dichloromethane and purified by column chromatography (CombiFlash $R_f$ automated column system; 40 g HP silica; eluted with a gradient of 0−100% EtOAc in hexanes) to afford the product **1** as a white solid (1.49 g, 50%, $R_f$: 0.25, TLC in 25% EtOAc in hexanes/$KMnO_4$ staining). $^1$H NMR (300 MHz, $CDCl_3$, 25 °C) $\delta$: 5.08 (s, 2H), 3.18 (s, 4H), 1.40 (s, 18H). $^{13}$C NMR (75 MHz, $CDCl_3$, 25 °C)


dx.doi.org/10.1021/ic302225z | Inorg. Chem. 2012, 51, 12575−12589

δ: 156.28, 79.19, 40.68, 28.28. HR-ESI-MS calcd. for $[C_{12}H_{24}N_2O_4+Na]^+$: 261.1814; found: 261.1814.

***N,N′*-Propargyl-*N,N′*-*tert*-butoxycarbonyl-1,2-diaminoethane (2).** **1** (500 mg, 1.92 mmol) was suspended in dry acetonitrile (20 mL, distilled over $CaH_2$ in house) and sodium *tert*-butoxide (462 mg, 4.80 mmol, 2.5 equiv) was added. The white suspension colored immediately to yellow. The suspension was cooled (0 °C) and propargyl bromide (1242 μL, 0.5 mmol, 6 equiv) in dry acetonitrile (5 mL) was added dropwise over 5−10 min. The reaction mixture darkened to light orange during the addition. Tetrabutyl ammonium iodide (TBAI) (1.4 g, 2 equiv) was added and the reaction mixture was left to stir, warming to room temperature as the ice water bath melted. TLC revealed the 100% consumption of starting material ($R_f$: 0.45, TLC in 40% EtOAc in hexanes) in favor of product ($R_f$: 0.65) after 48 h. Sodium *tert*-butoxide was filtered out and rinsed well with acetonitrile, and the combined filtrate was concentrated in vacuo to dryness. The resulting orange oil was dissolved in dichloromethane (5 mL) and the mixture was filtered over a short silica plug, rinsing well with dichloromethane (50 mL) to elute the toxic propargyl bromide. The filtrate was set aside and the silica was washed with ethyl acetate (50 mL). The ethyl acetate eluent was concentrated in vacuo to dryness and the resulting yellow oil was purified by column chromatography (CombiFlash $R_f$ automated column system; 24 g HP silica; eluted with a gradient of 0−50% EtOAc in hexanes) to afford the product **2** as a yellow solid (485 mg, 75%, $R_f$: 0.65, TLC in 40% EtOAc in hexanes/$KMnO_4$ staining). $^1$H NMR (300 MHz, $CDCl_3$, 25 °C) δ: 4.02 (d, 4H), 3.44 (s, 4H), 2.18 (s, 2H), 1.42 (s, 18H). $^{13}$C NMR (75 MHz, $CDCl_3$, 25 °C) δ: 154.49, 80.19, 79.22, 71.67, 43.98, 36.40, 28.08. HR-ESI-MS calcd. for $[C_{18}H_{28}N_2O_4+H]^+$: 337.2127; found: 337.2127, $[M+H]^+$.

***N,N′*-Propargyl-1,2-diaminoethane (3).** To a solution of **2** (134 mg, 0.40 mmol) in dichloromethane (2 mL) was added trifluoroacetic acid (TFA, 1 mL), and the yellow solution darkened to orange. The reaction mixture was stirred for 1 h at ambient temperature and then concentrated in vacuo to dryness. The resulting brown oil was dissolved in saturated $NaHCO_3$ (2 mL), and the resulting aqueous layer was extracted using dichloromethane (25 × 1 mL) until the extractions stained only faintly by TLC with $KMnO_4$ staining. The combined organic layers were dried ($Na_2SO_4$), filtered, and concentrated in vacuo to dryness. The resulting orange oil **3** was carried onto the next step without further purification (47 mg, 87%). $^1$H NMR (300 MHz, $CDCl_3$, 25 °C) δ: 3.45 (s, 4H), 2.85 (s, 4H), 2.22 (s, 2H), 1.77 (s, 2H). $^{13}$C NMR (75 MHz, $CDCl_3$, 25 °C) δ: 82.07, 71.20, 47.49, 37.82. HR-ESI-MS calcd. for $[C_8H_{12}N_2+H]^+$: 137.1079; found: 137.1076, $[M+H]^+$.

***N,N′*-[6-(Methoxycarbonyl)pyridin-2-yl]methyl-*N,N′*-propargyl-1,2-diaminoethane (4).** To a solution of **3** (196 mg, 1.43 mmol) in dry acetonitrile (9 mL, distilled over $CaH_2$) was added methyl 6-(bromomethyl)picolinate[28] (695 mg, 3.02 mmol, 2.1 equiv) and sodium carbonate (320 mg, 3.02 mmol, 2.1 equiv). The reaction was stirred at ambient temperature. Reaction monitoring by TLC revealed the formation and consumption of a singly alkylated intermediate ($R_f$: 0.50, TLC in 10% MeOH in DCM/UV activity) and formation of product ($R_f$: 0.55). After 48 h, sodium carbonate was filtered out, and the filtrate was concentrated in vacuo to dryness. The resulting brown oil was purified by column chromatography (CombiFlash $R_f$ automated column system; 24 g HP silica; eluted with a gradient of 0−10% MeOH in DCM) to afford the product **4** as a yellow solid (387 mg, 62%, $R_f$: 0.55, TLC in 10% MeOH in DCM/UV activity). $^1$H NMR (300 MHz, $CDCl_3$, 25 °C) δ: 7.96 (d, 2H), 7.71 (m, 4H), 3.94 (s, 6H), 3.90 (s, 4H), 3.42 (s, 4H), 2.71 (s, 4H), 2.18 (s, 2H). $^{13}$C NMR (75 MHz, $CDCl_3$, 25 °C) δ: 165.82, 160.12, 147.37, 137.34, 125.99, 123.60, 78.51, 73.34, 60.17, 52.86, 51.03, 42.84. HR-ESI-MS calcd. for $[C_{24}H_{26}N_4O_4+H]^+$: 435.2032; found: 435.2030, $[M+H]^+$.

***N,N′*-[1-Benzyl-1,2,3-triazole-4-yl]methyl-*N,N′*-[6-(carboxy)-pyridin-2-yl]-1,2-diaminoethane ($H_2$azapa·2HCl·1.5$H_2O$) (5·2HCl·1.5$H_2O$).** **4** (300 mg, 0.69 mmol, 1 equiv) was suspended in 1:1 *tert*-butanol/water, and benzyl azide (172 μL, 1.38 mmol, 2 equiv) was carefully added using precautionary blast shield protection and a plastic-tipped autopipet to prevent a friction-induced explosion. Sodium ascorbate (27 mg, 0.14 mmol, 0.2 equiv) was added, followed by copper(II) acetate monohydrate (276 mg, 1.38 mmol, 2 equiv). The suspension turned dark brown on addition of copper(II) acetate, but over 4 h the solid gradually dissolved and the solution lightened to blue-green. The reaction mixture was stirred at ambient temperature overnight (16 h) after which time a light blue-green precipitate was observed. The suspension was concentrated in vacuo to dryness. The resulting light blue-green solid was dissolved in 1:1 THF/water (50 mL) and sodium sulfide (829 mg, 3.5 mmol, 5 equiv) was added. A brown solid precipitated immediately, and the suspension was left to stir at ambient temperature for 24 h. The brown solid was filtered out using a fine fritted filter and the colorless filtrate was concentrated in vacuo to dryness. The resulting colorless solid was dissolved in a minimum volume of water and prepurified using a Waters C18 Sep-Pak 6 cc Vac cartridge (1 g sorbent, 55−100 μm particle size, gradient: 100% water to 50% MeOH/water to 100% MeOH) in 6−8 small portions. The cartridge was conditioned with methanol (2 × 2 mL) and water (2 × 2 mL) before each use. UV activity was confirmed in the 50% MeOH/water fractions by TLC before they were combined and concentrated in vacuo to dryness. The partially purified white solid was purified by semipreparative HPLC (A: 0.1% TFA, B: 100% MeCN, 0−100% B over 25 min, $t_R$ (broad) 15.7−18.0 min, 50 mg injections) to afford the product **5**·TFA as a white crystalline solid (272 mg, 44% based on 2 TFA per molecule). $^1$H NMR (300 MHz, MeOD, 25 °C) δ: 8.18 (s, 2H), 7.87 (m, 4H), 7.49 (d, 2H), 7.24 (s, 10H), 5.49 (s, 4H), 4.39 (s, 8H), 3.56 (s, 4H). $^{13}$C NMR (75 MHz, MeOD, 25 °C) δ: 167.30, 155.86, 148.58, 140.68, 139.99, 136.54, 130.17, 129.80, 129.39, 128.17, 127.66, 125.80, 58.24, 55.14, 50.98, 50.20. The synthesis was continued to form the HCl salt of $H_2$azapa. **5**·TFA (272 mg, 0.30 mmol) was dissolved in acetonitrile (3 mL). 0.1 M HCl (10 mL) was added, and the resulting solution was concentrated in vacuo to dryness. This procedure was repeated 4−5 times to afford the white solid **5**·2HCl·1.5$H_2O$ which was dried under high vacuum for several days before use (removal of TFA confirmed via $^{19}$F NMR). NMR structural assignments were confirmed using two-dimensional NMR experiments (Supporting Information, Figures S13−S14). $^1$H NMR (600 MHz, $D_2O$, 25 °C) δ: 7.57 (d, 2H; *H*3), 7.53 (s, 2H; *H*5), 7.41 (t, 2H, *H*4), 6.90 (m, 12H; *H*11, Ph*H*), 5.13 (s, 4H: *H*12), 3.37 (s, 4H: *H*9), 3.34 (s, 4H, *H*7), 2.26 (s, 4H, *H*8). $^{13}$C NMR (150 MHz, $D_2O$, 25 °C) δ: 172.67 (*C*1), 157.18 (*C*10), 153.12 (*C*4), 143.63 (*C*6), 138.09 (*C*2), 134.90 (*C*13), 128.98 (*C*15), 128.58 (*C*16), 128.00 (*C*14), 125.17 (*C*11), 124.85 (*C*5), 122.49 (*C*3), 59.73 (*C*9), 53.73 (*C*12), 50.37 (*C*8), 48.42 (*C*7). HR-ESI-MS calcd. for $[C_{36}H_{36}N_{10}O_4+H]^+$: 673.2999; found: 673.3000, $[M+H]^+$. Anal. Calcd. (found) for $C_{36}H_{36}N_{10}O_4$·2HCl·1.5$H_2O$: C, 55.96 (56.06); H, 5.35 (5.23); N, 18.13 (18.11).

**Metal Complexation Experiments: General Procedure.** $H_2$azapa·2HCl·1.5$H_2O$ (~0.015 mmol) was suspended in 0.1 M HCl (1.5 mL), and the appropriate metal chloride or perchlorate (1.2 equiv) was added. The pH was adjusted to 4−5 using 0.1 M NaOH, and then the solution was stirred at 60 °C. Any remaining solid dissolved upon heating. The reaction was stirred overnight (24 h), maintaining the same temperature.

**[Cu(azapa)].** $H_2$azapa·2HCl·1.5$H_2O$ (13.8 mg, 0.018 mmol) was reacted with copper(II) chloride dihydrate (3.7 mg, 0.0215 mmol, 1.2 equiv). After 24 h, a light blue precipitate was filtered out and purified by semipreparative HPLC (gradient: A: water, B: MeCN, 0−100% B over 25 min, $t_R$ (broad) 16.2−17.5 min) to afford the product [Cu(azapa)] as a green solid. HR-ESI-MS calcd. for $[C_{36}H_{34}{}^{63}CuN_{10}O_4+Na]^+$: 756.1958; found: 756.1951, $[M+Na]^+$. Anal. Calcd. (found) for $C_{36}H_{34}CuN_{10}O_4$·1.5$H_2O$: C, 56.80 (56.88); H, 4.90 (4.81); N, 18.40 (18.38).

**[Ga(azapa)][$ClO_4$].** $H_2$azapa·2HCl·1.5$H_2O$ (9.7 mg, 0.013 mmol) was reacted with gallium(III) perchlorate hexahydrate (7.2 mg, 0.015 mmol, 1.2 equiv). After 24 h, a white crystalline precipitate was filtered out to afford [Ga(azapa)][$ClO_4$]. NMR structural assignments were confirmed using two-dimensional NMR experiments (Supporting Information, Figures S18 and S19). $^1$H NMR (600 MHz, DMSO-$d_6$, 25 °C) δ: 8.65 (t, 2H; *H*4), 8.34 (m, 4H; *H*3, *H*11), 8.20 (d, 2H; *H*5),

7.32 (m, 10H; PhH), 5.65 (q, 4H; H12, H12′), 4.74 and 4.28 (2d, 4H; H7, H7′, $^2J$ = 18 Hz), 4.00 and 3.92 (2d, 4H; H9, H9′, $^2J$ = 15 Hz), 3.10 (m, 4H; H8, H8′). $^{13}$C NMR (150 MHz, DMSO-$d_6$, 25 °C) δ: 162.35 (C1), 150.57 (C6), 146.52 (C4), 143.58 (C2), 137.69 (C10), 135.74 (C13), 128.84 (PhC), 128.43 (C5), 128.24 (PhC), 127.94 (PhC), 127.10 (C11), 123.47 (C3), 56.31 (C7), 52.99 (C12), 47.80 (C8), 46.01 (C9). HR-ESI-MS calcd. for $[C_{36}H_{34}{}^{69}GaN_{10}O_4]^+$: 739.2020; found: 739.2014, $[M]^+$.

**[In(azapa)(H$_2$O)][ClO$_4$].** H$_2$azapa·2HCl·1.5H$_2$O (9.8 mg, 0.013 mmol) was reacted with indium(III) perchlorate hexahydrate (8.5 mg, 0.015 mmol, 1.2 equiv). After 24 h, a white crystalline precipitate was filtered out to afford the product [In(azapa)(H$_2$O)][ClO$_4$]. $^1$H NMR (400 MHz, DMSO-$d_6$, 25 °C) δ: 8.54−6.87 (br m, 18H), 5.49 (br s, 4H) 4.80−4.18 (m, 4H), 2.84 (s, 2H), 2.24 (s, 2H). $^1$H NMR (400 MHz, DMSO-$d_6$, 135 °C) δ: 8.19 (m, 4H), 7.98 (s, 2H), 7.57 (s, 2H), 7.29 (m, 6H), 7.12 (m, 4H), 5.42 (s, 4H), 3.93 (s, 4H), 3.66 (s, 4H), 2.59 (s, 4H). HR-ESI-MS calcd. for $[C_{36}H_{34}{}^{115}InN_{10}O_4]^+$: 785.1803; found: 785.1806, $[M]^+$.

**[Lu(azapa)][ClO$_4$].** H$_2$azapa·2HCl·1.5H$_2$O (9.8 mg, 0.013 mmol) was reacted with lutetium(III) chloride hexahydrate (6.1 mg, 0.015 mmol, 1.2 equiv). After 4 h the product was confirmed via mass spectrometry, and the solvent was removed in vacuo to yield [Lu(azapa)][ClO$_4$]. $^1$H NMR (300 MHz, D$_2$O, 25 °C) δ: 8.09 (br m, 2H), 7.98 (br m, 2H), 7.89 (s, 2H), 7.49 (br m, 2H), 7.31 (br m, 6H), 7.09 (br m, 4H), 5.32 (s, 4H) 4.14−3.91 (m, 6H), 3.65 (br m, 2H), 2.80−2.72 (m, 4H). $^{13}$C NMR (400 MHz, D$_2$O, 25 °C) δ: 172.52, 157.86, 150.34, 142.96, 134.38, 129.25, 129.03, 128.4, 125.63, 125.51, 124.06, 59.70, 54.73, 54.41, 52.99, 49.08. HR-ESI-MS calcd. for $[C_{36}H_{34}{}^{175}LuN_{10}O_4]^+$: 845.2172; found: 845.2166 $[M]^+$.

**X-ray Crystallography.** A small blue prism crystal of [Cu(azapa)] having approximate dimensions of 0.10 × 0.41 × 0.45 mm was grown by slow evaporation of a saturated solution in 1:1 MeCN/H$_2$O. A brown plate crystal of [In(azapa)(H$_2$O)][ClO$_4$]·2.5H$_2$O having approximate dimensions of 0.10 × 0.22 × 0.27 mm was grown by slow evaporation of a saturated solution in 1:1 MeOH/DMSO. The crystals were mounted onto respective glass fibers, and measurements were made on a Bruker Apex DUO diffractometer at −183 °C with graphite-monochromated Mo−Kα radiation. All data were collected and integrated using the Bruker SAINT[63] software package. Data were corrected for adsorption effects, and Lorentz and polarization effects using the SADABS[64] program. The structures were solved by direct methods using the SIR97[65] software and refined using SHELXL-97[66] via the WinGX[67] interface. [In(azapa)][ClO$_4$] crystallizes with 3 molecules of water in the crystal lattice. A summary of crystallographic data is presented in Table 1 for [In(azapa)(H$_2$O)][ClO$_4$] and in Table 2 for [Cu(azapa)]. CIF files for the two complexes as well as relevant bond lengths and angles are found in the Supporting Information.

**$^{67}$Ga/$^{111}$In Radiolabeling.** For $^{67}$Ga radiolabeling experiments, a 1 mg/mL stock solution of H$_2$azapa was made by dissolving 1.8 mg in 1.8 mL NaOAc buffer (10 mM, pH 4) with mild heat and vortex-mixing. An aliquot of chelator stock (750 μL) was transferred to a 20 mL sterile vial, and $^{67}$GaCl$_3$ (10 μL, ∼5 mCi) solution was added followed by NaOAc buffer (1.785 mL, 10 mM, pH 4) up to a total chelator concentration of 0.3 mg/mL. $^{111}$In labeling was performed similarly, with $^{111}$InCl$_3$ (15 μL, ∼6 mCi) and NaOAc buffer (1.240 mL, 10 mM, pH 5) being added to an aliquot of chelator stock solution (495 μL). The mixtures were agitated briefly and then allowed to react for 10 min at ambient temperature. The radiometal complex solutions were analyzed by analytical RP-HPLC (linear gradient A: 0.05% TFA, B: MeCN, 0−100% B over 20 min) to determine radiolabeling yields through peak integration: [$^{67}$Ga(azapa)]$^+$ $t_R$ = 12.8 min, >99%; [$^{111}$In(azapa)]$^+$ $t_R$ = 11.4 min, >99%. The retention times for the radioactive metal complexes determined by the Raytest NaI (Tl) detector were confirmed by analyzing the fully characterized nonradioactive metal complexes by RP-HPLC using the PDA detector: [Ga(azapa)]$^+$ $t_R$ = 12.7 min; [In(azapa)]$^+$ $t_R$ = 11.4 min.

**$^{177}$Lu/$^{64}$Cu Radiolabeling.** For $^{177}$Lu experiments, the chelators H$_2$azapa, DTPA, and DOTA were all dissolved up to 1 mg/mL in NaOAc buffer (10 mM, pH 5.0) as stock solutions. DTPA and H$_2$azapa required heating at 37 °C and frequent vortexing for 1−2 h to dissolve. Aliquots of each chelator stock solution were transferred to Corning 2.0 mL self-standing microcentrifuge tubes containing ∼1.2 mCi of $^{177}$Lu to a concentration of ∼182 mM, and made up to 1 mL with NaOAc buffer (10 mM, pH 5.0). H$_2$azapa and DTPA were allowed to radiolabel at ambient temperature for 10 min, and DOTA was radiolabeled for 1 h at 90 °C. Radiometal complexes were then evaluated using radio-HPLC (linear gradient A: 0.1% TFA in H$_2$O, B: MeCN, 0−80% B over 30 min): [$^{177}$Lu(azapa)]$^+$ $t_R$ = 19.3 min, >99%; [$^{177}$Lu(DOTA)]$^-$ $t_R$ = 6.8 min, >99%, [$^{177}$Lu(DTPA)]$^{2-}$ $t_R$ = 5.2 min, >99%. $^{64}$Cu labeling was performed in a similar manner with H$_2$azapa and DOTA at the same chelator concentrations previously used for labeling with $^{177}$Lu (182 mM) and with ∼800−1000 μCi of $^{64}$Cu. DOTA was radiolabeled at 90 °C for 60 min, and H$_2$azapa in 10 min at ambient temperature, and both were evaluated by RP-HPLC [$^{64}$Cu(azapa)] $t_R$ = 20.9 min, >99%; [$^{64}$Cu(DOTA)]$^{2-}$ $t_R$ = 7.1 min, >99%.

**$^{67}$Ga/$^{111}$In Mouse Serum Competition Experiments.** Frozen mouse serum was allowed to thaw for 30 min, and 750 μL of [$^{67}$Ga(azapa)]$^+$ solution was added in triplicate to 20 mL sterile vials containing 1250 μL of thawed mouse serum and 500 μL of PBS. The solutions sat at ambient temperature, and 800 μL aliquots were removed from each vial at 15 min, 1 h, and 2 h time points and diluted to a final volume of 2.5 mL with PBS in sterile vials. A 500 μL aliquot of [$^{111}$In(azapa)]$^+$ was added in triplicate to 20 mL sterile vials containing 750 μL of thawed mouse serum and 250 μL of PBS. The solutions were allowed to sit at ambient temperature, and 750 μL aliquots were removed at 1 and 24 h time points, and diluted to a final volume of 2.5 mL with PBS in sterile vials. The activities were counted, and the diluted mouse serum competitions were immediately loaded onto conditioned PD-10 size-exclusion columns. The 2.5 mL loading volumes were eluted and discarded into dedicated $^{111}$In or $^{67}$Ga radioactive waste containers, and the columns were then eluted with an additional 3.5 mL of PBS, which was collected into fresh 20 mL sterile vials. The activities of the eluents, which contained trans-chelated metal ions bound/associated with serum proteins, were counted and compared with the activity values obtained exactly prior to column loading to determine the percent radiometal ions that had been retained on the column as chelate-bound activity.

**$^{177}$Lu/$^{64}$Cu Blood Serum Competition Experiments.** Frozen human blood serum thawed for 30 min, and 750 μL aliquots were transferred to 2.0 mL Corning centrifuge vials. 300 μL of each $^{177}$Lu(chelator) was transferred to the blood serum, along with 450 μL of PBS to a total volume of 1.5 mL (in triplicate for each chelator). The final $^{177}$Lu(chelate) concentration present in serum was ∼36 mM. Serum competition samples were then incubated at 37 ± 0.1 °C with constant agitation (550 rpm) and analyzed via PD-10 size-exclusion column elution (filters MW < 5000 Da) at 1.5 and 24 h time points and counted using a Capintec CRC-15R dose calibrator. 750 μL of each serum/$^{177}$Lu(chelator) competition solution (in triplicate) was removed from the competition vial, diluted to 2.5 mL with PBS, and counted. The diluted aliquot of serum competition mixture was loaded onto a conditioned PD-10 column. The loading volume (2.5 mL) was eluted into radioactive waste, and then an additional 3.5 mL of PBS was loaded, collected, and counted in the dose calibrator as the serum-bound $^{177}$Lu (nonchelate bound). Percent stability was reported as a percentage of $^{177}$Lu still chelate-bound and not associated with serum proteins (MW < 5000 Da). Human serum competitions with $^{64}$Cu were performed in an identical fashion as described above for $^{177}$Lu, but with time points of 1 and 20 h.

**$^{64}$Cu Biodistribution Studies.** Biodistribution studies evaluated the basic stability and clearance of the $^{64}$Cu complexes of the commonly used chelator DOTA, and the novel entrant H$_2$azapa. Although the chelator NOTA is also widely used with $^{64}$Cu, and is known to be superior to DOTA in terms of in vivo stability and radiolabeling kinetics, DOTA was used as an initial first benchmark because of its wide availability and common use (currently used in 2 of 3 $^{64}$Cu-based clinical trials), and its superior properties with the isotopes $^{111}$In and $^{177}$Lu used in this study.[9,19,68] DOTA and H$_2$azapa were radiolabeled with $^{64}$Cu under the same conditions as described

above, and prepared for biodistribution studies in healthy nude athymic mice (female, 6−8 weeks old). The $^{64}$Cu(chelate) complexes were purified via RP-HPLC, concentrated in vacuo to dryness, and then suspended in 2:1 sterile saline 0.9% NaCl:PBS (pH 7) to a concentration and dose of ∼30 μCi in 200 μL per mouse (specific activity ∼10 μCi/μg, ∼ 3 μg $^{64}$Cu(chelate) per mouse). Each mouse was intravenously injected through the tail vein and sacrificed by $CO_2$ inhalation at time points of 15 min, 1 h, 4 h, and 24 h ($n$ = 4). Tissues collected after sacrifice included blood, heart, lungs, liver, spleen, kidneys, large intestine, small intestine, muscle, bone (femur), and skin. All organs were rinsed in water after removal and air-dried for 5 min. Tissues were weighed and counted (calibrated for $^{64}$Cu), the counts were background- and decay-corrected from the time of injection and then converted to the percentage of injected dose (%ID) per gram of organ tissue (%ID/g). The $^{64}$Cu counts measured in each organ were converted to activity using a calibration curve created from known standards of $^{64}$Cu.

**Small-Animal $^{64}$Cu-PET Imaging.** PET imaging was performed using a micro-PET R4 rodent scanner (Concord Microsystems) to visually confirm biodistribution results and monitor clearance of $^{64}$Cu. Two healthy, nude athymic mice (female, 6−8 weeks old) were administered doses of ∼300 μCi in 200 μL of 2:1 sterile saline (0.9% NaCl):PBS (pH 7) via intravenous tail vein injection (specific activity ∼10 μCi/μg, ∼30 μg of [$^{64}$Cu(azapa)] per mouse). Approximately 5 min prior to PET image acquisition, mice were anesthetized via inhalation of 2% isoflurane (Baxter Healthcare, Deerfield, IL)/oxygen gas mixture, placed on the scanner bed, and anesthesia was maintained during imaging using a reduced 1% isoflurane/oxygen mixture. Images were acquired at time points 1 h, 4 h, and 24 h, with PET data being recorded via static scans with a minimum of 10 million coincident events (30−60 min). An energy window of 350−700 keV and a coincidence timing window of 6 ns were used. Data were sorted into 2D histograms by Fourier rebinning, and transverse images were reconstructed by filtered back-projection (FBP) into a 128 × 128 × 63 (0.72 × 0.72 × 1.3 mm$^3$) matrix. The image data were normalized to correct for nonuniformity of response of the PET, dead-time count losses, positron branching ratio, and physical decay to the time of injection, but no attenuation, scatter, or partial-volume averaging correction was applied. The counting rates in the reconstructed images were converted to activity concentrations (percentage injected dose [%ID] per gram of tissue) by use of a system calibration factor derived from the imaging of a mouse-sized water-equivalent phantom containing $^{64}$Cu. Images were analyzed using ASIPro VM software (Concorde Microsystems).

## ■ ASSOCIATED CONTENT

### Ⓢ Supporting Information

Crystallographic information files (CIF) for the X-ray crystal structures along with relevant distance and bond angle data, $^{1}$H/$^{13}$C NMR spectra of all synthesized compounds, two-dimensional HSQC and HMBC NMR spectra of $H_2$azapa and [Ga(azapa)]$^+$, and HPLC radio-traces confirming quantitative radiolabeling of $H_2$azapa with all four radiometals. This material is available free of charge via the Internet at http://pubs.acs.org.

## ■ AUTHOR INFORMATION


### Corresponding Author

*Phone: (604) 222-7527 (M.J.A.), (604) 822-4449 (C.O.). Fax: (604) 222-1074 (M.J.A.), (604) 822-2847 (C.O.). E-mail: adam@triumf.ca (M.J.A.), orvig@chem.ubc.ca (C.O.).

### Author Contributions

‖These authors contributed equally to this work.


### Notes

The authors declare no competing financial interest.

## ■ ACKNOWLEDGMENTS

We acknowledge Nordion (Canada) and the Natural Sciences and Engineering Research Council (NSERC) of Canada for grant support, NSERC for CGS-M/CGS-D fellowships (E.W.P.) and a summer USRA scholarship (G.A.B), the University of British Columbia for 4YF fellowships (E.B. and E.W.P.), and Kuntalkumar Sevak from MSKCC (Lewis Lab) for skillful tail-vein injections of [$^{64}$Cu(azapa)]. C.O. acknowledges the Canada Council for the Arts for a Killam Research Fellowship (2011−2013).

## ■ REFERENCES


(1) Zeglis, B. M.; Lewis, J. S. *Dalton Trans.* **2011**, *40*, 6168−6195.
(2) Wadas, T. J.; Wong, E. H.; Weisman, G. R.; Anderson, C. J. *Chem. Rev.* **2010**, *110*, 2858−2902.
(3) Jones-Wilson, T. M.; Motekaitis, R. J.; Sun, Y.; Anderson, C. J.; Martell, A. E.; Welch, M. J. *Nucl. Med. Biol.* **1995**, *22*, 859−868.
(4) Laforest, R.; Dehdashti, F.; Lewis, J. S.; Schwarz, S. W. *Eur. J. Nucl. Med. Mol. Imaging* **2005**, *32*, 764−770.
(5) Blower, P. J.; Lewis, J. S.; Zweit, J. *Nucl. Med. Biol.* **1996**, *23*, 957−980.
(6) Anderson, C. J.; Ferdani, R. *Cancer Biother. Radiopharm.* **2009**, *24*, 379−393.
(7) Novak-Hofer, I.; Schubiger, A. *Eur. J. Nucl. Med. Mol. Imaging* **2002**, *29*, 821−830.
(8) McQuade, P.; Miao, Y.; Yoo, Y.; Quinn, T. P.; Welch, M. J.; Lewis, J. S. *J. Med. Chem.* **2005**, *48*, 2985−2992.
(9) Boswell, C. A.; Sun, X.; Niu, W.; Weisman, G. R.; Wong, E. H.; Rheingold, A. L.; Anderson, C. J. *J. Med. Chem.* **2004**, *47*, 1465−1474.
(10) Sun, X.; Wuest, M.; Weisman, G. R.; Wong, E. H.; Reed, D. P.; Boswell, C. A.; Motekaitis, R.; Martell, A. E.; Welch, M. J.; Anderson, C. J. *J. Med. Chem.* **2002**, *45*, 469−477.
(11) Sprague, J. E.; Peng, Y.; Sun, X.; Weisman, G. R.; Wong, E. H.; Achilefu, S.; Anderson, C. J. *Clin. Cancer. Res.* **2004**, *10*, 8674−8682.
(12) Clifford, T.; Boswell, C. A.; Biddlecombe, G. B.; Lewis, J. S.; Brechbiel, M. W. *J. Med. Chem.* **2006**, *49*, 4297−4304.
(13) Lee, F. T.; Mountain, A. J.; Kelly, M. P.; Hall, C.; Rigopoulos, A.; Johns, T. G.; Smyth, F. E.; Brechbiel, M. W.; Nice, E. C.; Burgess, A. W.; Scott, A. M. *Clin. Cancer Res.* **2005**, *11*, 7080s−7086s.
(14) Vandenbulcke, K.; Vos, F.; Offner, F.; Philippé, J.; Apostolidis, C.; Molinet, R.; Nikula, T.; Bacher, K.; Gelder, V.; Vral, A.; Lahorte, C.; Thierens, H.; Dierckx, R.; Slegers, G. *Eur. J. Nucl. Med. Mol. Imaging* **2003**, *30*, 1357−1364.
(15) Camera, L.; Kinuya, S.; Garmestani, K.; Wu, C.; Brechbiel, M. W.; Pai, L. H.; McMurry, T. J.; Gansow, O. A.; Pastan, I.; Paik, C. H.; Carrasquillo, J. A. *J. Nucl. Med.* **1994**, *35*, 882−889.
(16) Nayak, T.; Regino, C.; Wong, K.; Milenic, D.; Garmestani, K.; Baidoo, K.; Szajek, L.; Brechbiel, M. *Eur. J. Nucl. Med. Mol. Imaging* **2010**, *37*, 1368−1376.
(17) Woodin, K. S.; Heroux, K. J.; Boswell, C. A.; Wong, E. H.; Weisman, G. R.; Niu, W.; Tomellini, S. A.; Anderson, C. J.; Zakharov, L. N.; Rheingold, A. L. *Eur. J. Inorg. Chem.* **2005**, *2005*, 4829−4833.
(18) Wei, L.; Ye, Y.; Wadas, T. J.; Lewis, J. S.; Welch, M. J.; Achilefu, S.; Anderson, C. J. *Nucl. Med. Biol.* **2009**, *36*, 277−285.
(19) Cooper, M. S.; Ma, M. T.; Sunassee, K.; Shaw, K. P.; Williams, J. D.; Paul, R. L.; Donnelly, P. S.; Blower, P. J. *Bioconjugate Chem.* **2012**, *23* (5), 1029−1039.
(20) Ferdani, R.; Stigers, D. J.; Fiamengo, A. L.; Wei, L.; Li, B. T. Y.; Golen, J. A.; Rheingold, A. L.; Weisman, G. R.; Wong, E. H.; Anderson, C. J. *Dalton Trans.* **2012**, *41*, 1938−1950.
(21) Stigers, D. J.; Ferdani, R.; Weisman, G. R.; Wong, E. H.; Anderson, C. J.; Golen, J. A.; Moore, C.; Rheingold, A. L. *Dalton Trans.* **2009**, *39*, 1699−1701.
(22) Kotek, J.; Lubal, P.; Hermann, P.; Cisarova, I.; Lukes, I.; Godula, T.; Svobodova, I.; Taborsky, P.; Havel, J. *Chem.—Eur. J.* **2003**, *9*, 233−248.

(23) Nguyen, K.; Parry, J. J.; Rogers, B. E.; Anderson, C. J. *Nucl. Med. Biol.* **2012**, *39*, 187−197.
(24) Boros, E.; Ferreira, C. L.; Cawthray, J. F.; Price, E. W.; Patrick, B. O.; Wester, D. W.; Adam, M. J.; Orvig, C. *J. Am. Chem. Soc.* **2010**, *132*, 15726−15733.
(25) Ferreiros-Martinez, R.; Esteban-Gomez, D.; Platas-Iglesias, C.; Blas, A. d.; Rodriguez-Blas, T. *Dalton Trans.* **2008**, *42*, 5754−5765.
(26) Boros, E.; Ferreira, C. L.; Yapp, D. T. T.; Gill, R. K.; Price, E. W.; Adam, M. J.; Orvig, C. *Nucl. Med. Biol.* **2012**, *39*, 785−794.
(27) Boros, E.; Cawthray, J. F.; Ferreira, C. L.; Patrick, B. O.; Adam, M. J.; Orvig, C. *Inorg. Chem.* **2012**, *51*, 6279−6284.
(28) Price, E. W.; Cawthray, J. F.; Bailey, G. A.; Ferreira, C. L.; Boros, E.; Adam, M. J.; Orvig, C. *J. Am. Chem. Soc.* **2012**, *134*, 8670−8683.
(29) Boros, E.; Lin, Y.-H. S.; Ferreira, C. L.; Patrick, B. O.; Hafeli, U. O.; Adam, M. J.; Orvig, C. *Dalton Trans.* **2011**, *40*, 6253−6259.
(30) Boros, E.; Ferreira, C. L.; Patrick, B. O.; Adam, M. J.; Orvig, C. *Nucl. Med. Biol.* **2011**, *38*, 1165−1174.
(31) Mindt, T. L.; Struthers, H.; Brans, L.; Anguelov, T.; Schweinsberg, C.; Maes, V.; Tourwé, D.; Schibli, R. *J. Am. Chem. Soc.* **2006**, *128*, 15096−15097.
(32) Struthers, H.; Spingler, B.; Mindt, T. L.; Schibli, R. *Chem.—Eur. J.* **2008**, *14*, 6173−6183.
(33) Salvatore, R. N.; Shin, S. I.; Flanders, V. L.; Jung, K. W. *Tetrahedron Lett.* **2001**, *42*, 1799−1801.
(34) Nakon, R.; Angelici, R. J. *J. Am. Chem. Soc.* **1973**, *95*, 3170−3174.
(35) Liu, S.; Pietryka, J.; Ellars, C. E.; Edwards, D. S. *Bioconjugate Chem.* **2002**, *13*, 902−913.
(36) Hsieh, W.-Y.; Liu, S. *Inorg. Chem.* **2004**, *43*, 6006−6014.
(37) Liu, S.; He, Z.; Hsieh, W.-Y.; Fanwick, P. E. *Inorg. Chem.* **2003**, *42*, 8831−8837.
(38) Bartholoma, M. D.; Louie, A. S.; Valliant, J. F.; Zubieta, J. *Chem. Rev.* **2010**, *110*, 2903−2920.
(39) Malyarick, M. A.; Ilyuhin, A. B.; Petrosyants, S. P. *Main Group Met. Chem.* **1994**, *17*, 707−718.
(40) Maecke, H. R.; Riesen, A.; Ritter, W. *J. Nucl. Med.* **1989**, *30*, 1235−1239.
(41) Mindt, T. L.; Schweinsberg, C.; Brans, L.; Hagenbach, A.; Abram, U.; Tourwé, D.; Garcia-Garayoa, E.; Schibli, R. *ChemMedChem* **2009**, *4*, 529−539.
(42) Struthers, H.; Mindt, T. L.; Schibli, R. *Dalton Trans.* **2010**, *39*, 675−696.
(43) Tamanini, E.; Rigby, S. E. J.; Motevalli, M.; Todd, M. H.; Watkinson, M. *Chem.—Eur. J.* **2009**, *15*, 3720−3728.
(44) Lebedev, A. Y.; Holland, J. P.; Lewis, J. S. *Chem. Commun.* **2010**, *46*, 1706−1708.
(45) Bratsos, I.; Urankar, D.; Zangrando, E.; Genova-Kalou, P.; Kosmrlj, J.; Alessio, E.; Turel, I. *Dalton Trans.* **2011**, *40*, 5188−5199.
(46) Maisonial, A.; Serafin, P.; Traikia, M.; Debiton, E.; Thery, V.; Aitken, D. J.; Lemoine, P.; Viossat, B.; Gautier, A. *Eur. J. Inorg. Chem.* **2008**, *2008*, 298−305.
(47) Bastero, A.; Font, D.; Pericas, M. A. *J. Org. Chem.* **2007**, *72*, 2460−2468.
(48) Mirick, G. R.; O'Donnell, R. T.; DeNardo, S. J.; Shen, S.; Meares, C. F.; DeNardo, G. L. *Nucl. Med. Biol.* **1999**, *26*, 841−845.
(49) Connett, J. M.; Anderson, C. J.; Guo, L.-W.; Schwarz, S. W.; Zinn, K. R.; Rogers, B. E.; Siegel, B. A.; Philpott, G. W.; Welch, M. J. *Proc. Natl. Acad. Sci. U.S.A.* **1996**, *93*, 6814−6818.
(50) DeNardo, G. L.; Kukis, D. L.; Shen, S.; DeNardo, D. A.; Meares, C. F.; DeNardo, S. J. *Clin. Cancer Res.* **1999**, *5*, 533−541.
(51) Ferreira, C. L.; Yapp, D. T. T.; Crisp, S.; Sutherland, B. W.; Ng, S. S. W.; Gleave, M.; Bensimon, C.; Jurek, P.; Kiefer, G. E. *Eur. J. Nucl. Med. Mol. Imaging* **2010**, *37*, 2117−2126.
(52) Wadas, T. J.; Wong, E. H.; Weisman, G. R.; Anderson, C. J. *Curr. Pharm. Des.* **2007**, *13*, 3−16.
(53) Rogers, B. E.; Anderson, C. J.; Connett, J. M.; Guo, L. W.; Edwards, B.; Sherman, E. L. C.; Zinn, K. R.; Welch, M. J. *Bioconjugate Chem.* **1996**, *7*, 511−522.
(54) Anderson, C. J.; Connett, J. M.; Schwarz, S. W.; Rocque, P. A.; Guo, L. W.; Philpott, G. W.; Zinn, K. R.; Meares, C. F.; Welch, M. J. *J. Nucl. Med.* **1992**, *33*, 1685−1691.
(55) Zimmermann, K.; Grunberg, J.; Honer, M.; Amctamcy, S.; Schubiger, P. A.; Novak-Hofer, I. *Nucl. Med. Biol.* **2003**, *30*, 417−427.
(56) Bass, L. A.; Wang, M.; Welch, M. J.; Anderson, C. J. *Bioconjugate Chem.* **2000**, *11*, 527−532.
(57) Cole, W. C.; DeNardo, S. J.; Meares, C. F.; McCall, M. J.; DeNardo, G. L.; Epstein, A. L.; O'Brien, H. A.; Moi, M. K. *Int. J. Radiat. Appl. Instrum., Part B* **1986**, *13*, 363−368.
(58) Packard, A. B.; Kronauge, J. F.; Barbarics, E.; Kiani, S.; Treves, S. T. *Nucl. Med. Biol.* **2002**, *29*, 289−294.
(59) John, E. K.; Green, M. A. *J. Med. Chem.* **1990**, *33*, 1764−1770.
(60) Kelly, J. D.; Forster, A. M.; Higley, B.; Archer, C. M.; Booker, F. S.; Canning, L. R.; Chiu, K. W.; Edwards, B.; Gill, H. K.; McPartlin, M.; Nagle, K.; Latham, I.; Pickett, R.; Storey, A.; Webbon, P. *J. Nucl. Med.* **1993**, *34*, 222−227.
(61) Ando, A.; Ando, I.; Hiraki, T.; Hisada, K. *Int. J. Radiat. Appl. Instrum., Part B* **1989**, *16*, 57−80.
(62) McCarthy, D. W.; Shefer, R. E.; Klinkowstein, R. E.; Bass, L. A.; Margeneau, W. H.; Cutler, C. S.; Anderson, C. J.; Welch, M. J. *Nucl. Med. Biol.* **1997**, *24*, 35−43.
(63) *SAINT*, Version 7.68A; Bruker AXS Inc.: Madison, WI, 1997−2010.
(64) Riss, P. J.; Kroll, C.; Nagel, V.; Rösch, F. *Bioorg. Med. Chem. Lett.* **2008**, *18*, 5364−5367.
(65) Altomare, A.; Burla, M. C.; Camalli, M.; Cascarano, G. L.; Giacovazzo, C.; Guagliardi, A.; Moliterni, A. G. G.; Polidori, G.; Spagna, R. *SIR97*; *J. Appl. Crystallogr.*, Published Online **1999**.
(66) *SHELXTL*, Version 2008/4; Bruker AXS Inc.: Madison, WI, 2008;
(67) Farrugia, L. J. *WinGX*; *J. Appl. Crystallogr.*, Published Online **1999**.
(68) Schneider, D. W.; Heitner, T.; Alicke, B.; Light, D. R.; McLean, K.; Satozawa, N.; Parry, G.; Yoo, J.; Lewis, J. S.; Parry, R. *J. Nucl. Med.* **2009**, *50*, 435−443.